VISUALIZATION AND QUANTITATIVE ANALYSIS OF NUCLEAR SHUTTLING OF CARBOHYDRATE RESPONSE ELEMENT BINDING PROTEIN (CHREBP) IN PANCREATIC BETA CELLS

RASMUS GRØNNING

1. JANUAR 2018

UNIVERSITY OF SOUTHERN DENMARK
DEPARTMENT OF BIOCHEMISTRY AND MOLECULAR BIOLOGY

Abstract

The pancreas play a large part in maintaining energy homeostasis, though release of insulin from beta cells. A mechanism for detecting the glucose gradient is through a transcription factor; ChREBP, transcribing glycolysis and lipogenesis regulating genes. Using a viral construct ChREBP-EGFP is overexpressed in a mammalian beta cell line, allowing for visualization of through fluorescence microscopy. Calcium signaling, oscillations and nuclear translocation is investigated during glucose stimulation and removal of extracellular calcium. A selective FRAP analysis was performed by bleaching the nucleus and observing the recovery of signal, hereby allowing for the calculation of diffusion coefficients during fasting, feeding and in presence of a nuclear export inhibitor. A binding partner of ChREBP, named Mlx, was overexpressed and imaged with ChREBP, and investigated through Number & Brightness and TICS analysis.

Beta cells stimulated with glucose exhibited an increase in calcium oscillations of approximately 20-30%, while removal of extracellular calcium abolished calcium oscillations altogether. Translocation of ChREBP was not affected by removal of extracellular calcium. Selective FRAP recovery, was fit to a biexponential fit, which showed an immediate fast and subsequent slow recovery of cells. The rate constant was significantly lower in cells subjected to nuclear export inhibition during feeding. The number & brightness analysis showed that ChREBP and Mlx exist as a monomer in both nucleus and cytoplasm, during both feeding and fasting. Images acquired for TICS analysis contained too little signal to obtain a precise diffusion coefficient.

Preface and acknowledgment

Microscopy and work with cells were carried out at the Danish Molecular Biomedical Imaging Center (DaMBIC) at the Natural Science Faculty in University of Southern Denmark. Viral transductions were carried out in a Class II lab, on site. The ChREBP-EGFP viral construct along with the cell line INS-1E was donated from the Mandrup group. Special thanks to all the members of the Daniel Wüstner group, consisting of; Lab Technician Maria Smozek; PhD student Alice Dupont; Master students Thomas Bitsch and Selina Kruuse Hansen, for invaluable support with technical issues and feedback. Finally, the biggest thank you goes to Dr. Daniel Wüstner, for finding the time to help and provide guidance and support in the completion of this study.

Contents

Abbreviations

4-(2-hydroxyethyl)-1-piperazineethanesulfonic acid (HEPES)

Adenylyl-sulfate kinase (APK)

AMP-activated protein kinase (AMPK)

Carbohydrate Response Element (ChoRE)

Carbohydrate Response Element Binding Protein (ChREBP)

Chromosomal Maintenance 1 (CRM1)

Endoplasmatic reticulum (ER)

Enhanced Green Fluorescent protein (EGFP)

Fetal calf serum (FCS)

Flavin adenine dinucleotide (FAD)

Fluorescence correlation spectroscopy (FCS)

Inositol-1,4,5-triphosphate (IP_3)

Insulinoma-1E (INS-1E)

Leptomycin B (LMB)

Max-like protein (Mlx)

Nuclear Export signal (NES)

Nuclear Localization sequence (NLS)

Number & brightness analysis (N&B)

O-linked-N-acetylglucosamine modification (O-GlcNAc) transferase (OGT)

Phospholipase C (PLC)

Post Translational Modification (PTM)

Protein kinase A (PKA)

Protein phosphatase 2A (PP2A)

Purinergic G protein-coupled receptor 2 Y (P2Y)

Raster Image Correlation spectroscopy (RICS)

Region of interest (ROI)

Ryanodine Receptor (RyR)

Single particle tracking (SPT)

Stimulated Emission Depletion (STED)

Temporal image correlation analysis (TICS)

Turbo Red fluorescent protein (TurboRFP)

Voltage gated calcium channel (VGCC)

Xylulose-5-phosphate (X5P)

1. Introduction

Diabetes is a condition in which the regulation of blood glucose level is dysfunctional. According to a study by (Organization, 2016) 3,7 million deaths in 2012 were attributed to blood glucose levels being abnormal. The number of people affected by diabetes is increasing drastically, from 1980 to 2014 there was an increase of diabetic patients from 108 million to 442 million; a 4-fold increase and this growth is expected to continue. The global prevalence increased from 4.7% to 8.5% in the same timeframe. Treatment of diabetes is lifelong and very costly. It is estimated that diabetes cost the global economy 500 billion US$ in 2010 and is estimated to rise to at least 745 billion US$ in 2030 (Bloom et al., 2012). Two main types of diabetes exist; Type 1 and 2 (Organization, 2016). Type 1 is characterized by a low or lack of production of insulin, playing a key role in lowering the blood glucose level. Type 2 is characterized by the tissue becoming resistant to insulin signaling, typically caused by obesity. Untreated diabetes may lead to lower limb amputation, loss of vision, kidney failure or cardiovascular disease.

The main organ to regulate blood glucose is the pancreas, more specifically clusters of cells called pancreatic islets of Langerhans. These islets mediate the response by sensing the glucose level and releasing insulin. Around 20 % of the cells in pancreas are alpha cells, producing and secreting glucagon, elevating the blood glucose level. More prevalent are the beta cells which constitute 65-80% of the cells in pancreas, and secrete insulin which reduces the blood glucose level. The beta cells react to a high glucose level by sensing key metabolites which are needed to activate transcription factors of the central metabolic pathway. A significant transcription factor is Carbohydrate Response Element Binding Protein (ChREBP). ChREBP exist in two isoforms; ChREBPα (864 bp) and ChREBPβ (687 bp), the latter having a deletion of a low-glucose inhibitory domain (LID), two nuclear export signals (NES) and a nuclear localization signal (NLS) (Filhoulaud et al., 2013). ChREBP which has shuttled to the nucleus binds so-called Carbohydrate Response Elements (ChoRE), which lead to increased expression of the following genes. *Tx-NIP*, inducing apoptosis indicating a role in glucotoxicity and beta-cell loss (Minn, Hafele, & Shalev, 2005). *L-PK*, transcribing the L-type pyruvate kinase catalyzing the last step of glycolysis (da Silva Xavier, Rutter, Diraison, Andreolas, & Leclerc, 2006; Kawaguchi, Takenoshita, Kabashima, & Uyeda, 2001). *FAS*, catalyzes the synthesis of fatty acids (da Silva Xavier et al., 2006). ChREBP not only increases expression of target genes but also repress genes such as; *GcK*, a glucokinase which phosphorylates glucose to glucose-6-phosphate, providing a negative feedback loop for ChREBP activation (da Silva Xavier, Sun, Qian, Rutter, & Leclerc, 2010). Also repressed is the *Pdx-1* gene, transcribing a transcription factor necessary for beta-cell development and survival. *Pdx-1* works in combination with *MafA*, another gene repressed by ChREBP, to transcribe the

insulin gene (Aramata, Han, Yasuda, & Kataoka, 2005). The number of potential binding sites of ChREBP is estimated to be 74,967 in INS-1E cells based on the motif CACGTGn_5CACGTG (Schmidt et al., 2016).

1.1 Inhibition and activation of ChREBP

During fasting ChREBP is retained in the cytoplasm by a plethora of inhibitory mechanisms, including post translational modifications (PTMs) (fig. 1). One of these is phosphorylation of ChREBP at Ser-140 and Ser-192 by Protein Kinase A (PKA), promoted by glucagon (Dentin et al., 2012; Kabashima, Kawaguchi, Wadzinski, & Uyeda, 2003; Sakiyama et al., 2008). These phosphorylation's recruit the 14-3-3 protein, binding to ChREBP hereby providing cytosolic retention. AMP-activated protein kinase (AMPK) and Adenylyl-sulfate kinase (APK) phosphorylates Ser-568 and Thr-666, respectively, hereby inhibiting the DNA binding activity of ChREBP (Kawaguchi, Osatomi, Yamashita, Kabashima, & Uyeda, 2002). Abundance of free fatty acids results in an increased ChREBP mRNA decay (Dentin et al., 2005; Xu, Christian, & Jump, 2006). Activation of ChREBP-mediated response is initiated by increasing levels of glucose. Two metabolites are involved in the activation of ChREBP, one being xylulose-5-phosphate (X5P) and the other glucose-6-phosphate (G-6-P). The former; X5P, activates protein phosphatase 2A (PP2A), which removes all phosphorylation's hereby preventing the binding to 14-3-3 and restoring DNA binding capabilities (Kabashima et al., 2003). The latter; G-6-P, upregulates ChREBP transcriptional activity but the exact mechanism is not yet known (Dentin et al., 2012; Li et al., 2010). ChREBP continuously shuttles between cytoplasm and the nucleus, in presence of glucose the rate of nuclear entry is increased (Davies, O'Callaghan, & Towle, 2008; Dentin et al., 2012; Li et al., 2010). Nuclear entry of ChREBP is dependent on the recognition of a nuclear localization signal (NLS) by importin-α and importin-β, two nuclear transport proteins (Ge et al., 2011). Importin-α binds competitively with 14-3-3 to ChREBP, hereby regulating its import (Sakiyama et al., 2008). Activation of ChREBP can additionally require the PTM; O-linked-N-acetylglucosamine modification (O-GlcNAc) by O-GlcNAc transferase (OGT), which increases the expression and protein level of target genes (Guinez et al., 2011). Another PTM involved in activation of ChREBP is the acetylation of Lys-672 by p300, increasing the recruitment to promotor regions of the target genes (Bricambert et al., 2010). As the level of glucose drops, the signal from ChREBP is terminated through translocation to the cytoplasm by Chromosomal Maintenance 1 (CRM1), a nuclear export protein (Nguyen, Holloway, & Altura, 2012; Sakiyama et al., 2008). ChREBP is subsequently phosphorylated and retained in cytoplasm by 14-3-3. This is the classical pathway of activation of ChREBP, but there are additional mechanisms inhibiting or active activating ChREBP mediated transcription.

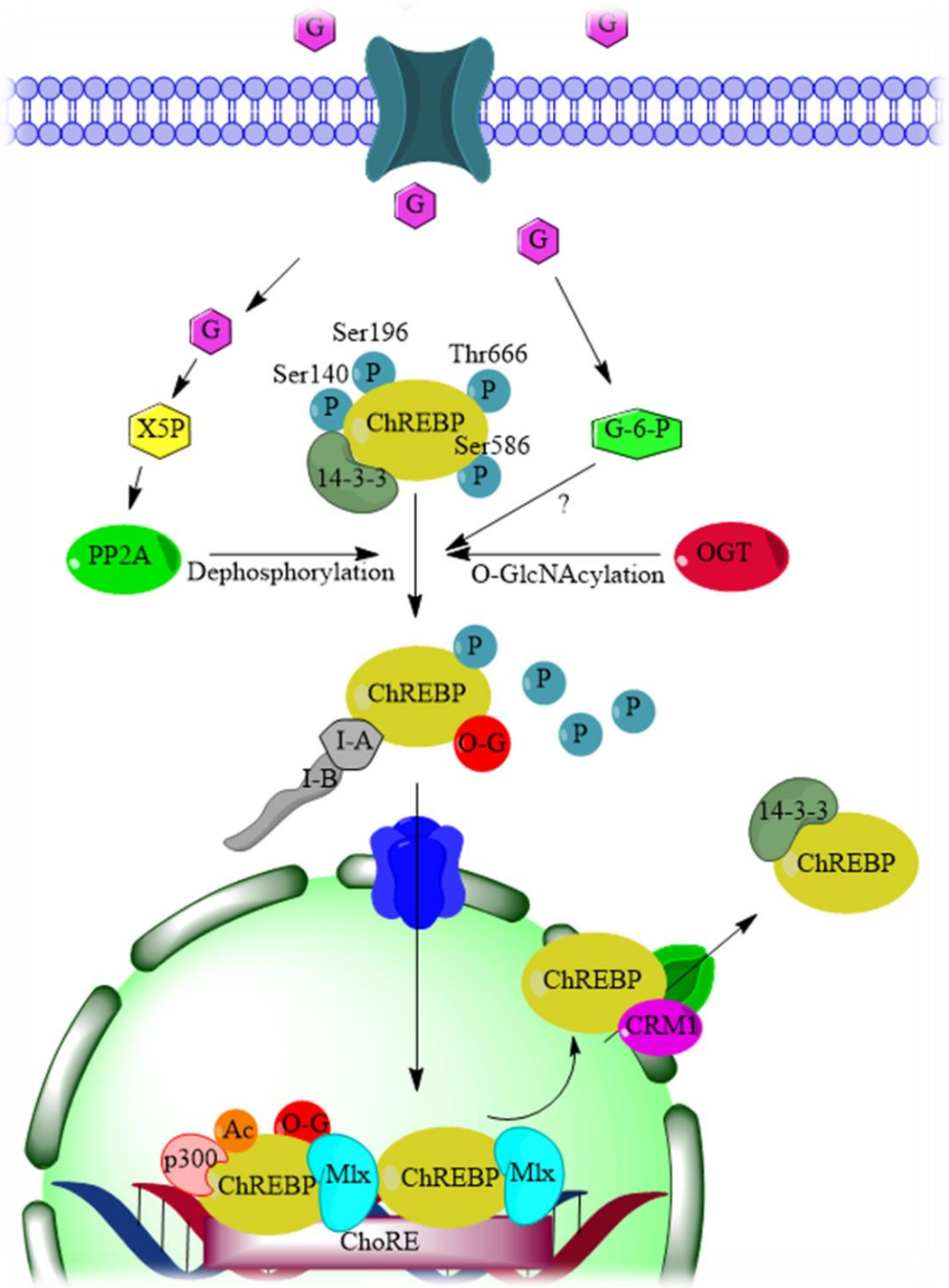

Figure 1 ChREBP is retained in its inactive state in the cytoplasm by 14-3-3 binding, due to PKA (ser140 and ser192) phosphorylation's. A decreased DNA binding capability is provided by AMPK (ser 586) and APK (thr666). Increasing xylullolose-5-phosphate (X5P) concentration activates protein phosphatase 2A (PP2A) dephosphorylation, removing 14-3-3 and allowing Importin-α/β (I-A/B) binding. Further activation comes from an O-linked-N-acetylglucosamine modification (O-G) by O-G transferase (OGT). Glucose-6-phosphate also activates ChREBP, but the mechanism is not fully elucidated. Two ChREBP/Mlx complexes assemble around a ChoRE region, and are acetylated by p300, allowing transcription of relevant genes. ChREBP is rendered inactive by phosphorylation and exported by Chromosomal Maintenance 1 (CRM1) and subsequently retained in the cytoplasm. Illustration is adapted from (Filhoulaud, Guilmeau, Dentin, Girard, & Postic, 2013; Havula & Hietakangas, 2012; Wang, Viscarra, Kim, & Sul, 2015) and created in ChemDraw 16.

1.2 Max-like protein interactions

A vast transcription factor network, Myc/Max/Mad, regulates cell size, differentiation, proliferation and apoptosis of many cell types. Another protein closely related to this network is Max-like protein (Mlx), binding to many of the same target genes such as Mad1, Mad4 and Mnt/Rox. A major difference however is the ability of Myc/Max to interact with one another or Mad, whereas Mlx does not interact with Max/Myc (Billin, Eilers, Queva, & Ayer, 1999; Meroni et al., 2000). The interaction between either Mlx/Mad or Max/Mad both lead to repression of CACGTG-dependent targets through Mad1, Mad4 and Mnt/Rox genes. Another common function of Mlx and Max is the ability to act as both a repressor and activator. Where Max either binds Mad/Myc to inhibit or activate transcription, respectively, Mlx either binds Mad or ChREBP also to inhibit or activate transcription. Interaction with ChREBP forms a heterodimer, which can bind and transcribe ChOREs (Ma, Tsatsos, & Towle, 2005). A ChoRE consists of two CACGTG-motifs separated by 5 basepairs, indicating that two Mlx/ChREBP heterodimers are needed to interact with the ChoRE (Ma, Sham, Walters, & Towle, 2007).

1.3 Calcium pathway

An important signalling molecule in cells are calcium ions Ca^{2+} from either internal calcium stores or extracellular media (Berridge et al., 2003). Increased cytoplasmic calcium concentration has long been known to promote insulin secretion, but also ChREBP activity is regulated by calcium. This response in beta-cells occurs through the uptake of glucose, its conversion to ATP, and subsequent activation of ATP sensitive potassium channels (fig. 2). The voltage change from pumping out K^+, leads to uptake of extracellular calcium through voltage gated calcium channels (VGCC). Internal calcium stores are typically activated by the activation of a G protein-coupled receptor. Purinergic G protein-coupled receptor 2 Y (P2Y) is an example of a receptor with affinity towards ATP. Upon ATP binding Phospholipase C (PLC) is activated and based on which of the six isotypes is stimulated the Ca^{2+} response varies, from small and slow response to a large rapid release of Ca^{2+}. PLC cleaves inositol phospholipid, creating inositol-1,4,5-triphosphate (IP_3) which activates inositol-1,4,5-triphosphate receptor (IP_3R) located in the endoplasmatic reticulum (ER), releasing Ca^{2+} to the cytosol. The Ryanodine Receptor (RyR), also located on ER, reponds to the increased Ca^{2+} level by releasing additional Ca^{2+} to the cytoplasm. As in many other cell types the internal calcium store in pancreatic beta-cells is located in the endoplasmatic reticulum (ER). From the ER, waves of calcium are continually released. Each wave is called an oscillation and there has been observed an oscillation pattern in beta-cells called “bursting”. A dual oscillator model has been proposed by (Bertram, Sherman, &

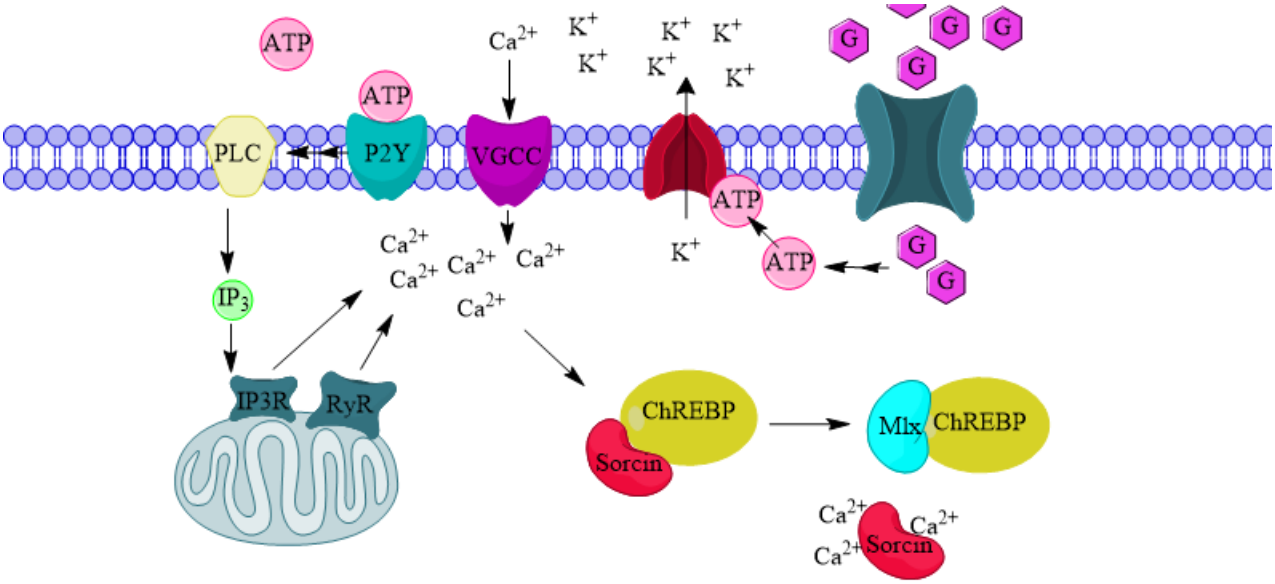

Figure 2 Increasing glucose (G) concentration, converted to ATP through glycolysis and oxidative phosphorylation, activates potassium (K^+) excretion, which leads to activation of a voltage gated calcium channel (VGCC) importing calcium into cytoplasm. Activation of purinergic G protein-coupled receptor 2Y (P2Y), activates phospholipase C (PLC) mediated cleavage of inositol-1,4,5-triphosphate (IP_3) and binding to inositol-1,4,5-triphosphate receptor (IP3R) located on ER, releases additional calcium to the cytoplasm, followed by Ryanodine Receptor (RyR) mediated calcium release, activated by increasing calcium concentration. Sorcin binding to ChREBP retains it in the cytoplasm, however binding of Sorcin to calcium changes its conformation, releasing ChREBP and allowing Mlx binding and nuclear translocation. Adapted from (Berridge, Bootman, & Roderick, 2003; Noordeen, Meur, Rutter, & Leclerc, 2012) and created in ChemDraw 16.

Satin, 2013) stating that fast oscillations are due to calcium feedback on potassium channels, while slower oscillations are linked to glycolysis. Calcium is linked to ChREBP activity through sorcin, a calcium binding protein, binding and retaining ChREBP it in the cytoplasm during low Ca^{2+} conditions(Noordeen et al., 2012). Release of calcium disrupts the Sorcin/ChREBP-binding allowing the latter to cross the nuclear envelope. Overexpression of sorcin retains ChREBP in the cytoplasm even during high glucose conditions, while sorcin-silencing results in a permanent ChREBP accumulation in the nucleus, even during low glucose conditions.

This study will investigate the effect of extracellular calcium and glucose stimulation on oscillations in a pancreatic beta cell line, named INS-1E. An overexpression of ChREBP will be carried out, through a transduction with an Adenoviral construct transcribing a fluorescent ChREBP. The location of this construct and its mobility will be investigated during feeding and fasting to verify its effect by glucose metabolites. Use of a nuclear export inhibitor will accumulate additional ChREBP in the nucleus, whether this affects mobility, nuclear translocation and binding of ChREBP will be determined. This will be done through the bleaching of all nuclear ChREBP fluorescence and observation of its recovery. The ChREBP construct will be co-expressed with its binding partner Mlx. Stoichiometry and diffusion coefficient of ChREBP and Mlx will be calculated through a number & brightness analysis and TICS, respectively, based on time lapse images in cytoplasm and nucleus, during feeding and fasting.

2. Materials and methods

2.1 Cell culture

A pancreatic beta cell line, insulinoma-1E (INS-1E) from Rattus Norvegicus was used for cell culture experiments. The growth media used was RPMI-1640 with Glutamax^{TM}. Additionally, NaPyruvate (1 mM), 5% Fetal Calf seruim (FCS), glucose (11 mM) and β-MeOH (50 µM) penicillin (100 U/mL) and streptomycin (100 mg/mL) was added. The cells were grown in an incubator with 5% CO_2 at 37^o C, and split 1:5 once a week, hereby keeping the cells at same confluency for each experiment. A 10-mL dish was used for general cell growth while Corning 35 mm culture dishes were used for microscopy (appendix 7.1).

2.2 Transduction

Overexpression of a full-length ChREBP was induced with a viral construct; Ad-CMV-EGFP-mChREBP donated by the Susanne Mandrup group (Boergesen et al., 2011). Viral construct (1 µl) was added directly to the plate with growth media and washed away after 2-hour incubation at 5% CO_2 at 37^o C on cells approximately 40 to 50% confluent. The construct was then allowed to be expressed for 18 hours in growth media containing 5 mM glucose. In some experiments conducted in high glucose (25 mM), a 45% glucose solution was added to the plate 3 hours before microscopy. Mlx overexpression was induced with an adenoviral construct, transcribing pAV[Exp]-CMV-Mlx-TurboRFP bought from Vectorbuilder (supplementary data 1). Virus (0,35 µl) was added to 30-40% confluent cells, washed away after 2 hours and incubated 48 hours at 5% CO_2 at 37^o C.

2.3 Live cell imaging of ChREBP-EGFP, Ca^{2+} and Mlx-TurboRFP

2.3.1 Calcium imaging

Imaging of calcium was made possible using the fluorophore Fluo-4-AM (Invitrogen), which binds free calcium in the cells and media. The microscope plates were incubated with Fluo-4 (4,5 µM) for 30 minutes at 5% CO_2 and 37^o C, and subsequently washed in M1 media containing either 1 mM $CaCl_2$ or no calcium. Imaging was carried out on a Leica DMIRB-E with a 63x/1.4 oil objective through widefield microscopy. Additional calcium experiments were carried out, overexpressing ChREBP in low (5mM) to high (25mM) glucose, in M1 media with or without calcium. Images were acquired before changes to the glucose gradient and 2 hours after, in the previous conditions described. The microscope used was a Zeiss LSM 510 with a 63x NA 1.4 oil objective, illuminated from an argon laser exciting the fluorophore at 488 nanometer (nm) with a laser power of 2 milliwatt (mW). Emission was collected at 500 to 550 nm and reflected light was collected in every wavelength and used to visualize the relative health of cells.

2.3.2 Nuclear accumulation with Leptomycin B

INS-1E cells expressing the ChREBP-EGFP construct was imaged either immediately after the addition of 5 ng/mL leptomycin B (LMB); a nuclear export inhibitor inhibiting CRM1. The cells incubated with LMB contained 11 mM glucose. Images were obtained on a motorized Nikon Ti-E microscope with a built-in Okolab microscope stage incubator allowing imaging at 37° C. A Yokogawa CSU-X1 spinning disk allowed very fast z-stack images through a 60x NA 1.4 objective. Laser power was set to 20 mW using 491 nm excitation and collection of emission from 525 to 539 nm.

2.3.3 Selective FRAP on ChREBP-EGFP

INS-1E cells expressing ChREBP-EGFP were washed and imaged with M1 media containing either 5 mM (low) or 25 mM (high) glucose, respectively. Additional samples were incubated 1 hour with 5 ng/ml LMB. Emission collection and objective was the same as described in 2.3.1. Laser power was set low to 0.375 mW to reduce bleaching. The nucleus was bleached with 30 mW for approximately 8 to 10 seconds, in a region covering only 70% of the nuclear space to reduce bleaching of cytoplasmic signal. A Tempcontrol 37-2 digital unit, was utilized to keep the cells at 37° C, for a closer mimic of physiological cell condition.

2.3.4 Mlx-TurboRFP and ChREBP-EGFP co-expression

Imaging of ChREBP-EGFP followed the standard protocol as described in section 2.3.3, except for a 63x NA 1.2 water objective being used, instead of 63x NA 1.4 oil. The laser intensity used to illuminate the Mlx-TurboRFP construct was 0,066 mW at 543 nm excitation. Emission was collected at 500 to 550 nm for EGFP and 565-615 nm for TurboRFP. Additional images were acquired on a Leica TCS SP8 to be used for quantitative analysis, using either two photomultiplier (PMT) detectors or one HyD photon counting detector. In the experiment using the two PMT detector both fluorophores were imaged using 509 nm excitation and collection of emission from 514 to 544 and 580 to 700 nm. This excitation at 509 nm wavelength was optimal for simultaneous excitation (fig. 3). Laser power was set to 16 mW, on a 63X NA 1.4 oil objective. Images acquired with the resonant scanner and HyD detector was excited in 488 nm and 553 nm for EGFP and TurboRFP, respectively. Their emission was collected from 498 to 543 nm and 564 to 738 nm with laser power set to 4 mW.

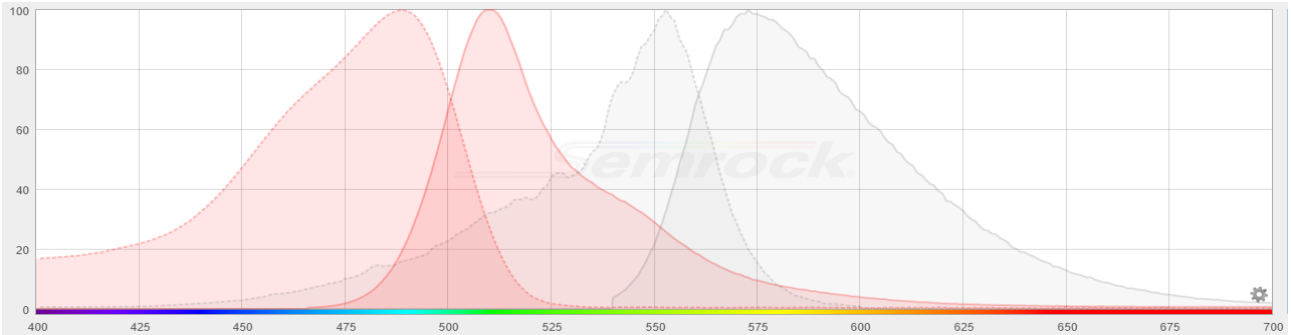

Figure 3 The emission (dotted) and excitation (firm) of EGFP (red) and TurboRFP (Blue) (Semrock.com).

2.4 Image analysis

2.4.1 Selection and measuring of cells

Cell regions were chosen based on multiple criteria; cells not growing 100% confluent or in layers; small number of apoptotic cells and finally; a high relative amount of fluorescence. A previous study did not indicate any functional difference between cells with low and high signal (supplementary data 2). The focus was adjusted so that the nucleus was at its largest diameter (fig. 4). Images acquired from microscopy were analyzed in ImageJ. Using the measure option, the integrated density was calculated from the area chosen and its mean grey value. Due to technical difficulties with the transduction, cells overexpressing ChREBP or Mlx, varied greatly in intensity (fig. 4B). The brightest cells, indicating the highest level of overexpression were chosen for imaging.

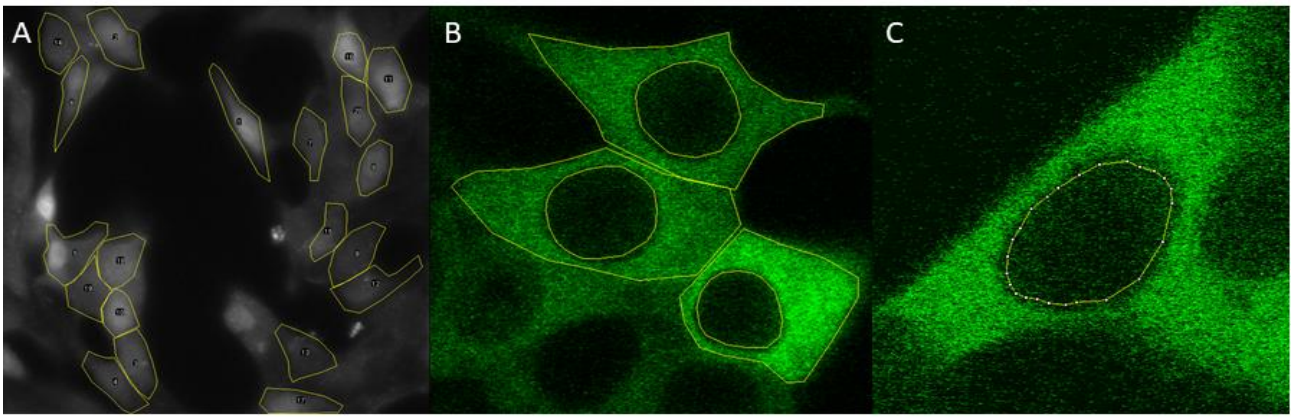

Figure 4 Examples of the selection of measured areas (yellow area), also called ROI. A) Measurement of calcium oscillation after glucose stimulation, using Fluo-4 B) ratio of nuclear vs total cell signal in a cell overexpressing ChREBP and C) measurement of nuclear signal after bleaching of ChREBP.

2.4.2 Selective FRAP analysis

Single cells with a clear outline were selected and imaged as described in the previous section 2.3.3 and 2.4.1 (fig 4C). An ROI covering the nucleus was used to measure the integrated density, and normalized to pre-bleach intensity using the equation

$$F_n(t) = \frac{F(t) - F_0}{F_{pre} - F_0}$$

See (fig. 5A) for visualization of the normalization. The average recovery from one biological replicate was calculated for each condition and plotted using the ImageJ function Curvefitter. By trial-and-error the best fit was found to be biexponential described by $y = a * (1 - \exp(-b * x)) + c * (1 - \exp(-d * x))$, where a and c are the amplitude of the first and second exponential uptake (fig.5B). The rate constants for the first and second fraction were described by b and d.

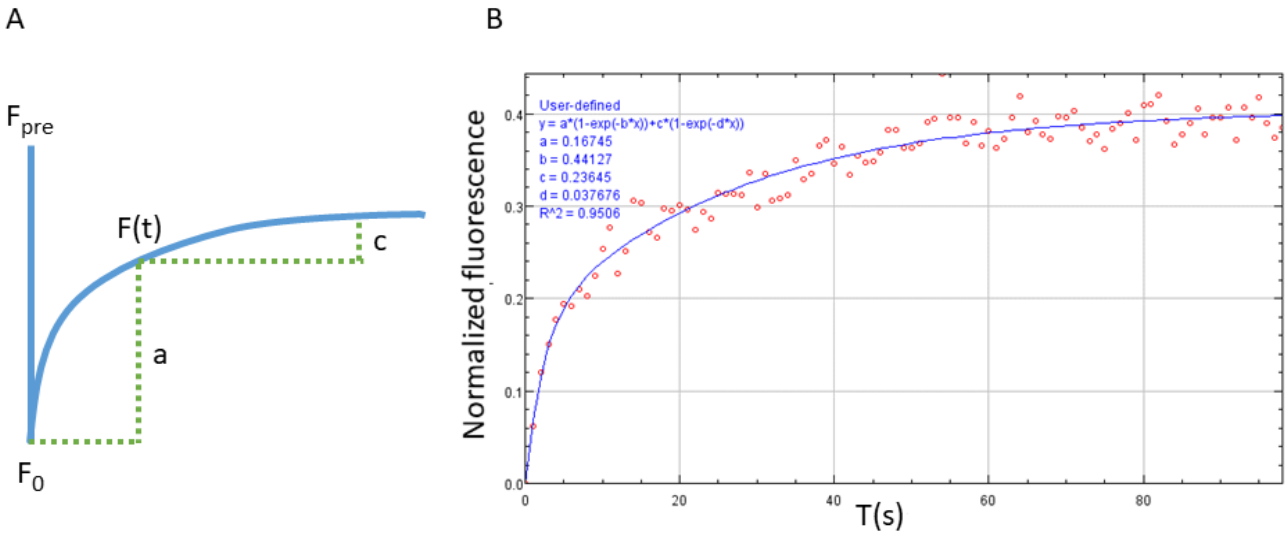

Figure 5 A) normalization of integrated density numbers from ROI recovery after bleaching. The recovery to a specific time (F(t) was normalized to the pre-bleach intensity (F_{pre}) using the post-bleach intensity (F_0). B) The amplitude (a,c) and rate constants (b,d) were calculated and plotted as a biexponential function using the ImageJ function; Curvefitter, using the average recovery from each condition in each replicate.

2.4.3 Fluorescence correlation spectroscopy

Fluctuations in fluorescence is analyzed through Fluorescence correlation spectroscopy (FCS), a method based on the observation that particles in a suspension move in random direction due to their collision with atoms or molecules. This movement is known as Brownian motion, and is the basis principle in FCS.

2.4.3.1 Number & Brightness analysis

A variant of FCS targeted against images was developed by (Digman, Dalal, Horwitz, & Gratton, 2008) called the Number & brightness analysis. This method provides a way to measure the apparent number of particles, using the number (N) analysis. The brightness (B) analysis can be used to calculate the amount of particles that aggregate, hereby determining the stoichiometry of a target protein. The equations used for N&B analysis is given by;

$$B = \frac{\sigma^2}{\langle k \rangle}$$

$$N = \frac{\langle k \rangle^2}{\sigma^2}$$

In the number & brightness analysis the brightness parameter (B) is calculated from the variance in intensity from one pixel to another. The variance is described by the letter sigma σ, which is given by two contributors. The first is the occupation number, meaning how many particles are in a given pixel. The second contributor to the variance is noise from the detector. Average intensity of the target protein is

given by (*k)* and is calculated as the number of particles in illumination focus times molecular brightness as photons emitted per second per molecule. To calculate the brightness, the square of variance (σ^2), is divided by the number of molecules (k). If the mean variance is 1 it indicates that the target protein exist entirely as a monomer. A mean variance of 2 would indicate that the target protein exist as a dimer or that half exist as a monomer, and the other half as a trimer, and so forth. Calculation of the number of molecules (N), is calculated as the number of molecules in focus (k) divided by (B) calculated previously. This expression is reduced to the square of number of molecules in focus (k) divided by the square of variance (σ^2). The value given by the N analysis provides a number of how many molecules are in each pixel on average. A macro written by Dr. Daniel Wüstner was used for automation of the raw calculations (Appendix 7.2).

2.4.3.2 TICS analysis

A different approach method utilizing FCS in images is temporal image correlation analysis (TICS) (Wiseman, Squier, Ellisman, & Wilson, 2000). This technique measures the average spatial correlation between images in a time lapse, hereby determining a time autocorrelation function. The autocorrelation function is based on how fast a number of fluorophores move through the focal volume. The spatial averaging is performed throughout the time lapse by comparing small regions of the image at one time to the same region or another region of the image, at a different time. The analysis runs until all regions have been compared to all other regions, at all given timepoints. A requirement of TICS is use of relatively photostable fluorophores, which also move slowly through the area given by the point spread function so that at least a few frames can be obtained of the same molecules.

An investigation by (Lund & Wustner, 2013) comparing single particle tracking (SPT) and TICS, determined that the diffusion coefficient is overestimated when large immobile fluorescent structures are present using TICS, and underestimated using (SPT). In both methods the transport parameters were affected by the signal-to-noise ratio. As previously mentioned, TICS excels in determining diffusion coefficient of slower diffusing proteins and protein aggregates. In a study by (Lund, Lomholt, Solanko, Bittman, & Wustner, 2012), TICS is used to calculate the diffusion coefficient of a very slow diffusing fluorescent cholesterol containing vesicle.

3. Results & discussion

3.1 Calcium imaging

3.1.1 Effect of glucose stimulation on beta cell oscillation

To verify that the cell line INS-1E was able to respond to glucose as described in literature, a series of experiments were conducted. Effect of calcium release was investigated in pancreatic beta cells by binding of calcium to Fluo-4, a fluorophore which increases its signal 100 times upon binding to calcium. Samples incubated with Fluo-4 were imaged every second for 400 seconds, and were stimulated with glucose after 100 images (supplementary data 3). The pancreatic cells were continually oscillating, but responded dramatically and simultaneously to an increase in glucose concentration by emitting more signal (fig. 6A-B). Measurement of the signal increase was carried out as described in section 2.4.1, in three biological replicates, consisting of 10, 14 and 20 technical replicates. To effectively determine how much of the response is due to the glucose stimulation, the post-stimulation values were normalized to the pre-stimulation values (fig. 6C). The peak of each calcium wave reached an approximate 20-30 % increase in total signal compared to pre-stimulation. Since the cells do not oscillate at the same time the amount of signal from each cell varies drastically from image to image. This is visualized through the size of the error lines describing the difference in obtained signal, relative to each cell. A more pronounced error line indicates a larger relative difference in cell signal whereas a lower error line would indicate cells have stopped oscillating. Due to technical difficulties in adding glucose, the distance from which the glucose was added to the plate, to where the cells where imaged, varied greatly. This is the most probable cause for the time variance between each replicate. Response to the glucose stimulation, corresponds with the hypothesis of sorcin mediated ChREBP retention, which hereby inhibits the sorcin/ChREBP binding allowing nuclear translocation.

3.1.2 Effect of extracellular calcium removal on beta cell oscillation

Beta-cells incubated with Fluo-4, were imaged in media without calcium, before change to calcium-rich media. The intensity of cells was calculated as described in section 2.4.1, and normalized to the intensity of the first image. Fluctuations in calcium signal were plotted as error lines as in (fig. 6C). The removal of calcium inhibited all oscillations (fig.7A), however reintroducing the same plate of cells to media with calcium, restored oscillations (fig7B). Imaging of cells during no-calcium conditions required a higher exposure time, resulting in more bleaching of the fluorophore. Exposure time remained the same during calcium and no-calcium conditions to keep the bleaching constant. Additional experiments were performed, in opposite conditions, first confirming oscillation in calcium-rich media, before change to no-calcium media, resulting in lack of oscillations (Data not shown).

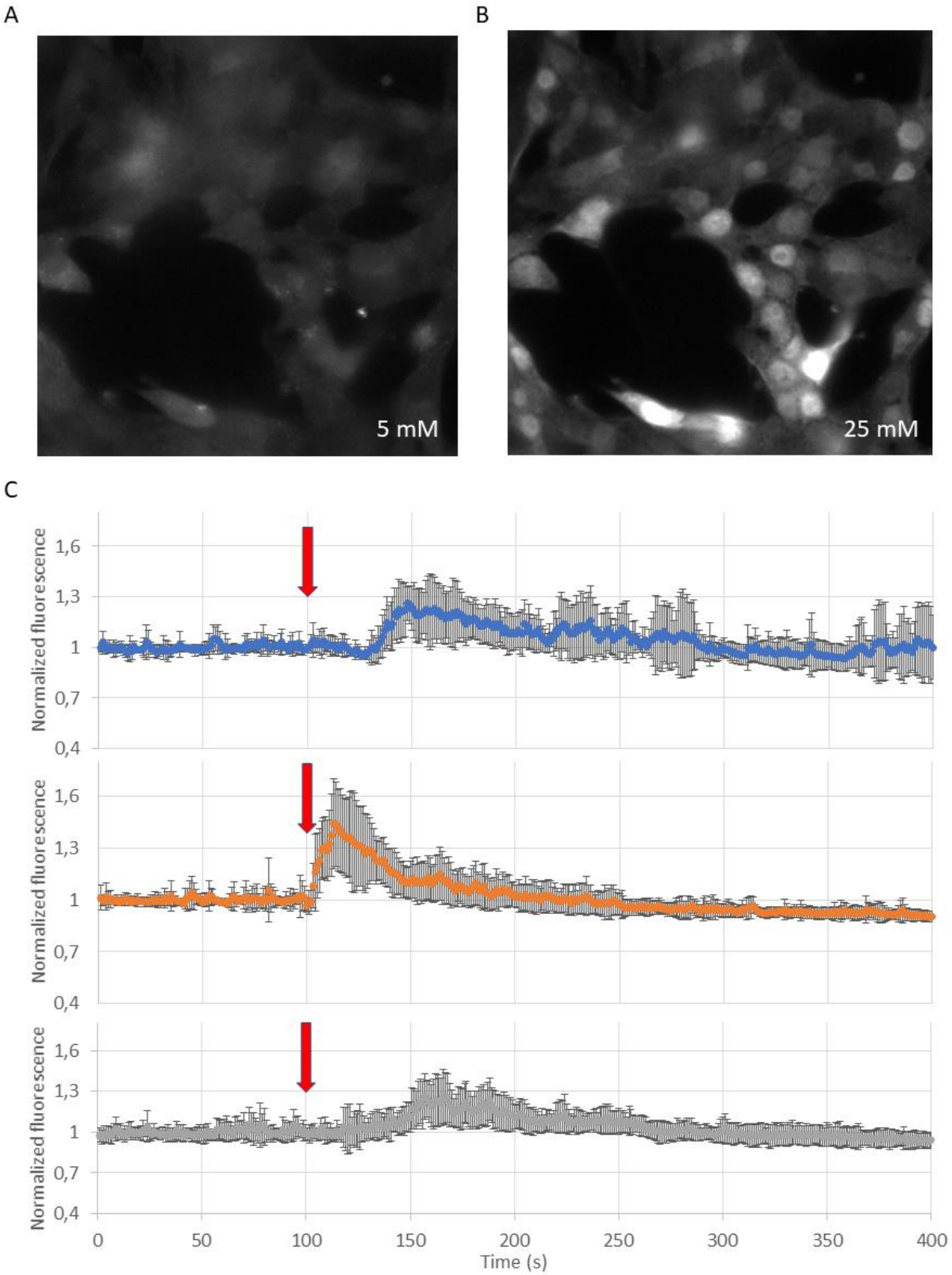

Figure 6 Example of calcium release in a beta cell before (A) and after (B) glucose stimulation, visualized by Fluo-4. C) Response of beta cells treated with Fluo-4, to glucose stimulation (5 mM to 25 mM) performed at t=100 seconds. The intensity of each cell was averaged and normalized to the pre-stimulation average. Glucose stimulation (red arrow), n= 10(blue), 14(orange), 20(grey).

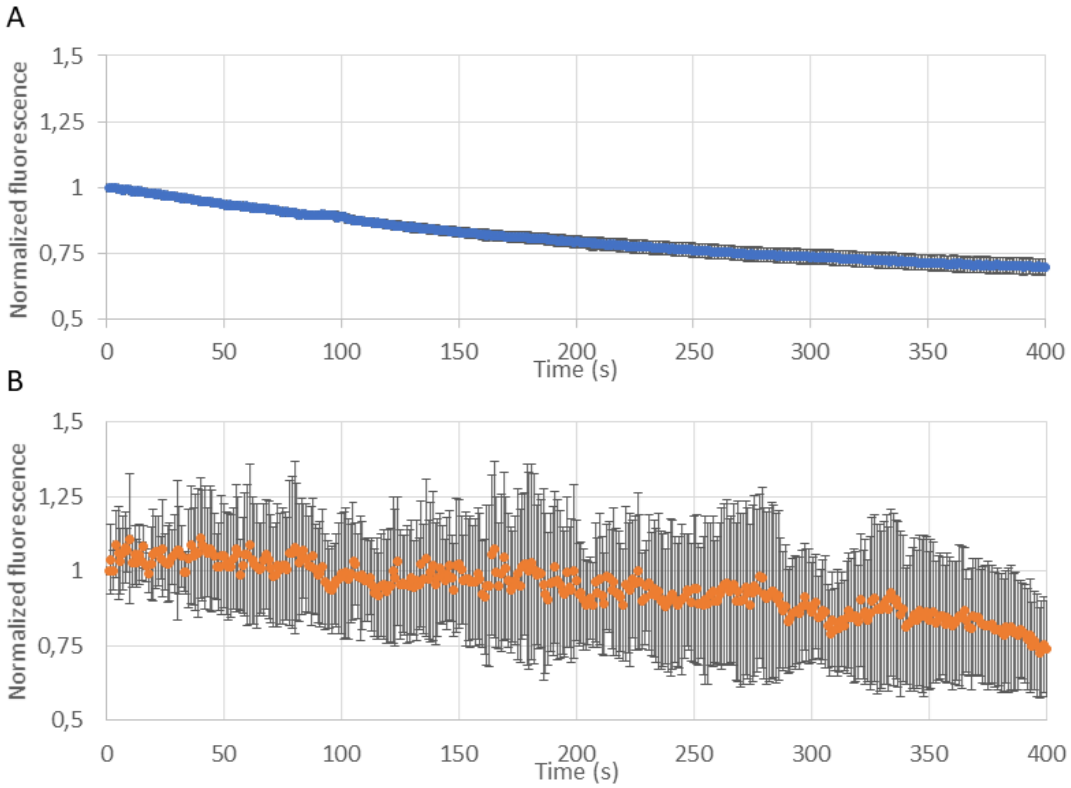

Figure 7 Oscillations in beta cells were investigated in media without (A) and with (B) calcium. Signal was normalized to the integrated density of the first frame (n=10). Error lines visualize the fluctuations in calcium.

3.1.3 Calcium dependency on nuclear ChREBP accumulation

Transport of ChREBP across the nuclear membrane was investigated during fasting and feeding, with and without calcium. Pancreatic beta cells overexpressing ChREBP were imaged in low glucose media (5 mM) before 2-hour incubation with high glucose (25 mM), and subsequent imaging. A ratio of nuclear signal versus total signal was calculated as described in section 2.4.1. This ratio showed an expected increase of ChREBP in the nucleus, approximately 2-fold (fig. 8). A similar ratio was calculated for cells incubated in low and high glucose, without calcium. Interestingly removal of calcium did not affect the accumulation of nuclear ChREBP, indicating that the intracellular pool of calcium is sufficient to inhibit the sorcin-mediated cytosolic retention of ChREBP. This result is contrasted by a study from (Noordeen et al., 2012). Herein the effect of extracellular calcium is investigated using EGTA, a calcium chelator removing extracellular calcium. Nuclear accumulation of ChREBP was unchanged on a 10-minute time scale, using EGTA in high glucose conditions. Interestingly a nuclear accumulation of ChREBP was observed 10 minutes after adding EGTA and ATP in high glucose conditions. Using EGTA and ATP in low glucose conditions did not yield a nuclear accumulation. Summarizing two studies; short term nuclear accumulation of ChREBP without extracellular

calcium is dependent on a high level of ATP and glucose, whereas long term nuclear accumulation is only dependent on a high level of glucose. The most likely explanation for the long term nuclear ChREBP accumulation is due to the production of ATP, from glucose through glycolysis and oxidative phosphorylation.

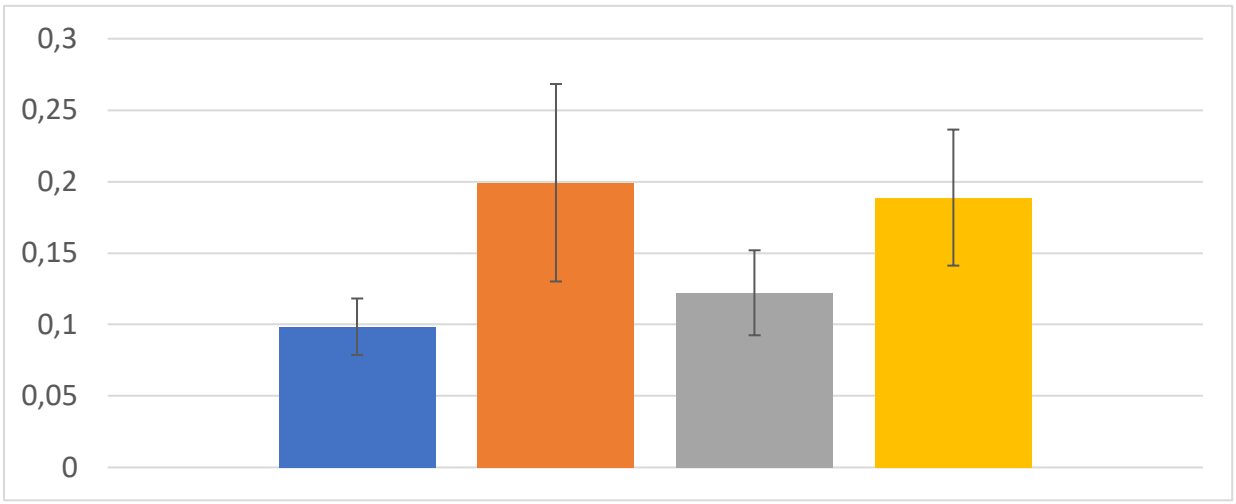

Figure 8 Ratio of nuclear/total ChREBP in beta cells during low (5 mM) (blue,grey) and high (25 mM) (orange,yellow) glucose conditions, with (blue,orange) or without (grey,yellow) calcium, respectively. Error lines are plotted as the standard deviation n=10.

3.2 Nuclear translocation analysis

ChREBP continually shuttles from cytoplasm to nucleus, feeding or fasting alike. By inhibiting the nuclear export, and bleaching all signal from the nucleus it can be determined the nuclear translocation is increased during feeding or fasting.

3.2.1 Inhibition of nuclear ChREBP export

To investigate nuclear translocation during feeding and fasting, LMB was used to inhibit the nuclear export of ChREBP, through the binding to the nuclear export factor CRM1, hereby increasing the level of nuclear ChREBP. Different concentrations (0,1;1;10 ng/mL) of LMB was previously used to verify the effect of export inhibition, and imaged after 1-hour incubation (supplementary data 2). A spinning disk microscope, as described in section 2.3.2, was used to acquire a time-lapse of nuclear accumulation (supplementary data 4). Using the function sum slices in ImageJ, combining the signal from the 5 images providing the largest nuclear area, the signal/noise ratio was improved drastically. A continuous nuclear accumulation of ChREBP was observed, based on visual evaluation. This indicates that 5 ng/mL is sufficient for CRM1 inhibition, and shuttling of ChREBP occurs in normal glucose conditions (fig. 9).

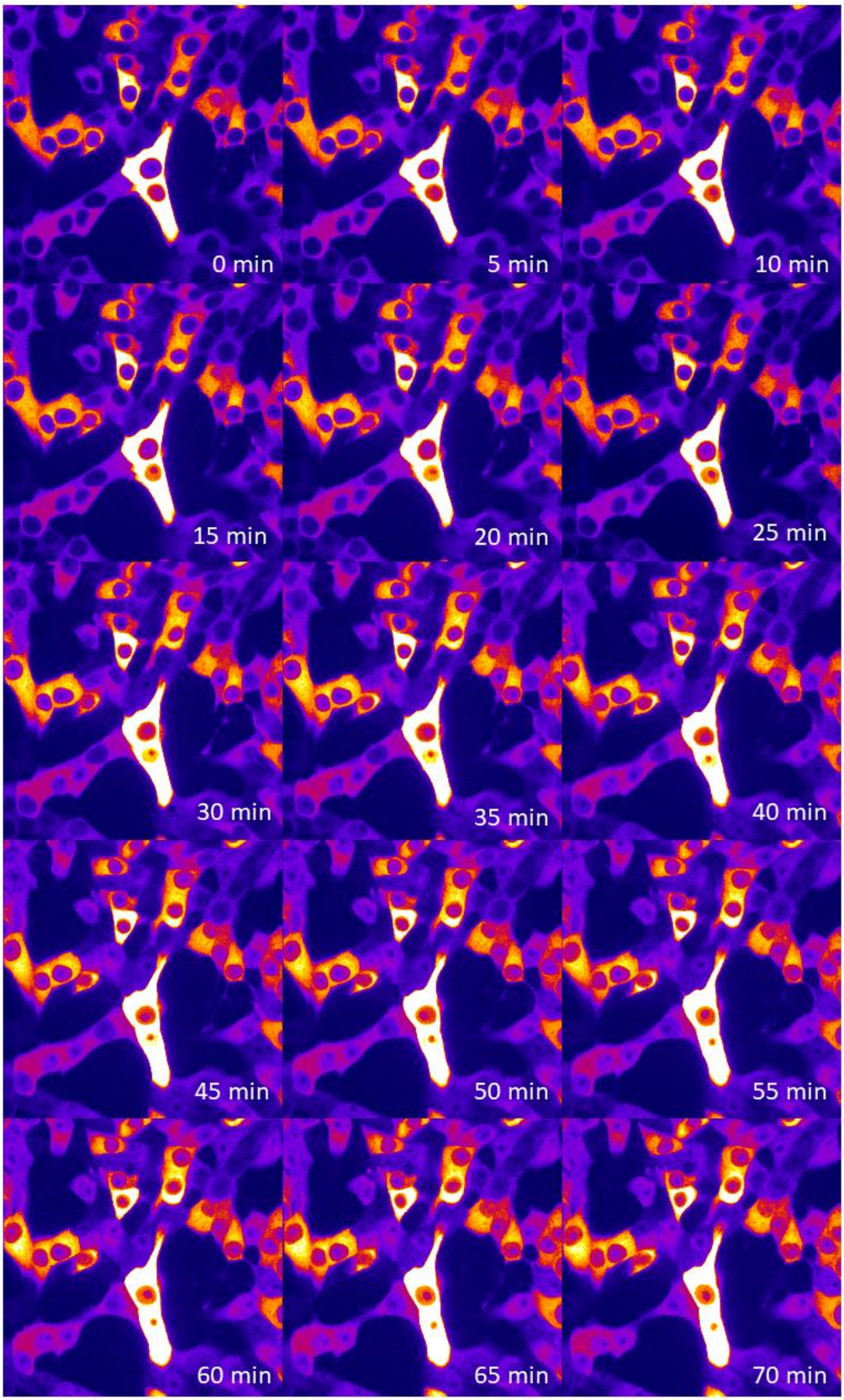

Figure 9 Nuclear accumulation of ChREBP, in pancreatic beta cells stimulated with LMB, imaged every 5 minutes. Each image is the sum of 5 images focusing on nucleus.

3.2.2 Selective-FRAP analysis

Nuclear translocation of ChREBP was investigated in four conditions during feeding or fasting, either with or without LMB. Using the image technique fluorescence recovery after photo-bleaching (FRAP) the entirety of nuclear envelopes were bleached with 30 mW laser power, and the recovery-region selected as described in section 2.4.1. Recovery was observed by acquiring one image every second for a total of 98 frames and calculated as described in section 2.4.2. Spontaneous recovery did not account for the observed recovery (supplementary data 5). The average intensity was calculated for 7 to 10 technical replicates yielding 1 averaged biological replication which was also averaged to other biological replications, totaling 3 biological replications (fig. 10A-B). A standard mean of error was calculated by averaging each biological replicate average to each other and plotted for each condition. Fitting the recovery to each individual averaged biological replicate, showed a biexponential fit in all 4 conditions (data not shown). A common trait of all recovery curves was the presence of a very fast exponential recovery followed by a slower exponential recovery. Hence the first and second exponential recovery are from here on, named as fast and slow, respectively. The amplitude, meaning the amount of signal observed in the fast fraction, was approximately 2-fold lower in cells treated with LMB relative to untreated (fig. 10C). The amplitude of the slower fraction also indicated an approximate 2-fold decrease in cells treated with LMB relative to non-treated (fig. 10D). Interestingly half of the total amplitude seems to be from the slow fraction, while the other half is from the fast fraction. Calculation of the rate constant of the slow recovery indicated a slight increase in cells treated with LMB during high glucose (fig. 10E). Additionally, the rate constant of the fast recovery was significantly lower for cells treated with LMB in high glucose, than cells treated with LMB in low glucose, or untreated cells in low and high glucose (fig. 10F).

There are multiple interpretations of why the amplitude might be lowered of cells in low and high glucose treated with LMB. One explanation could be that ChREBP fluctuate during feeding and fasting, and when the nuclear export is inhibited by LMB, ChREBP starts to accumulate. ChREBP is easily translocated to the nucleus due to its low amount relative to the cytoplasm. After some time with LMB treatment, the amount of ChREBP in the nucleus, being much higher than in untreated low and high glucose cells, will have to be transported into the nucleus towards a much higher concentration than previously, hereby inhibiting the nuclear translocation. A more likely explanation is that the amount of ChREBP is too low in the nucleus to obtain a high signal-to-noise ratio. As for the significantly decreased rate constant of the slow recovery in cells in high glucose condition treated with LMB, this might be cause by the nucleus being so “full” of ChREBP that the shuttling back and forth, normally observed have ceased. This is based on the observation that some cells seemed to contain the same amount of ChREBP in nucleus and cytoplasm alike.

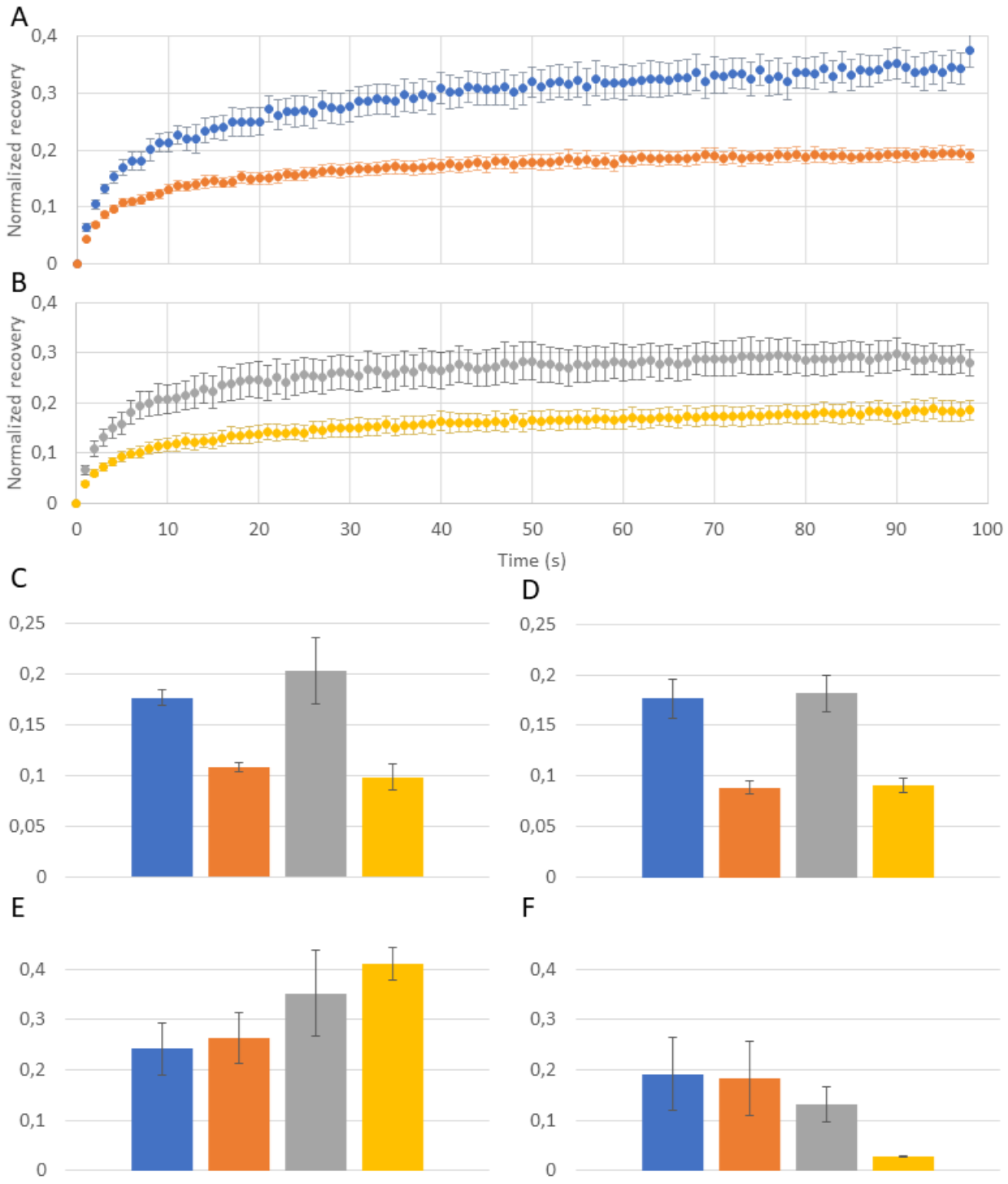

Figure 10 Recovery normalized to the prebleach intensity during low, 5 mM, (A; blue/orange) and high, 25 mM, (B; grey/yellow) glucose conditions. Additionally, LMB was added (orange/grey) to inhibit nuclear export. The recovery was fit to a biexponential recovery with a fast (C,E) and a slow (D,F) component. The amplitude was calculated an plotted (C,D), along with the rate constants (E,F) for each condition. The standard mean of error was calculated and added as error lines (N=3 n=7-10).

3.3 Co-expression of ChREBP and Mlx

3.3.1 Optimization of Mlx transduction

A viral construct transcribing Mlx-TurboRFP was to be expressed in INS-1E in combination with ChREBP-EGFP, preferably using the same protocol. In the first Mlx-transduction the beta-cells were subjected to 0.5; 1 and 2 µL virus. In all 3 conditions there was an elevated level of apoptotic cells and detachment of cells, clumping together and forming huge clusters, relative to the ChREBP transduction. The condition with the most attached cells and least apoptotic cells was the one with 0.5 µL virus (fig 11A1-3). It was speculated that the overexpression was leading the cells to detach and form these clusters due to pancreatic islet development, induced by the increased level of Mlx. This hypothesis was rejected using a control plasmid based on the same adeno-virus, expressing GFP instead of Turbo-RFP/Mlx. The resulting images from the transduction using 0.5; 1 and 2 µL virus all showed the same tendency of the cells to clump and form clusters multiple layers of cell thick (fig. 11B1-3). Coating of the microscope plates with collagen, the main structural protein in the extracellular space, and poly-D-lysine, which has a positive charge, binding negatively charged cells, did not have an effect on apoptosis and detachment (fig.11C1-3). Next the incubation time was changed from 18 hours to 42 hours, and the concentration of virus lowered to 0.15;0.25;0.5 µL. Adding less than approximately 0.5 µL virus is very difficult since the volume is so low, and it proved to be impossible to add 0,1 µL. This assessment was performed by pipetting the media containing the construct multiple times and determining whether there was a visual difference in the amount of liquid in the pipette tip. The lowest concentration of virus; 0.15 µL, provided healthy attached cells with a decent amount of signal, however most cells did not express the construct (fig. 12A1-3). Increasing virus concentration provided more signal in a larger number of cells, 0.5 µL signs of apoptosis in approximately half of cells (fig. 12B1-3). The cell passage number had reached a high number, which can affect the growth and survivability of cells, a new stock was therefore prepared. Subsequent transduction with 0.2 and 0.4 µL construct, and imaging showed a drastic improvement in cell viability and no to low clumping (fig. 12C1-3; 0.2 µL & D1-3; 0.4 µL). It was decided to use 0.35 µL viral construct in future experiments, since it was the lowest amount of virus that could be pipetted precisely, based on visual evaluation.

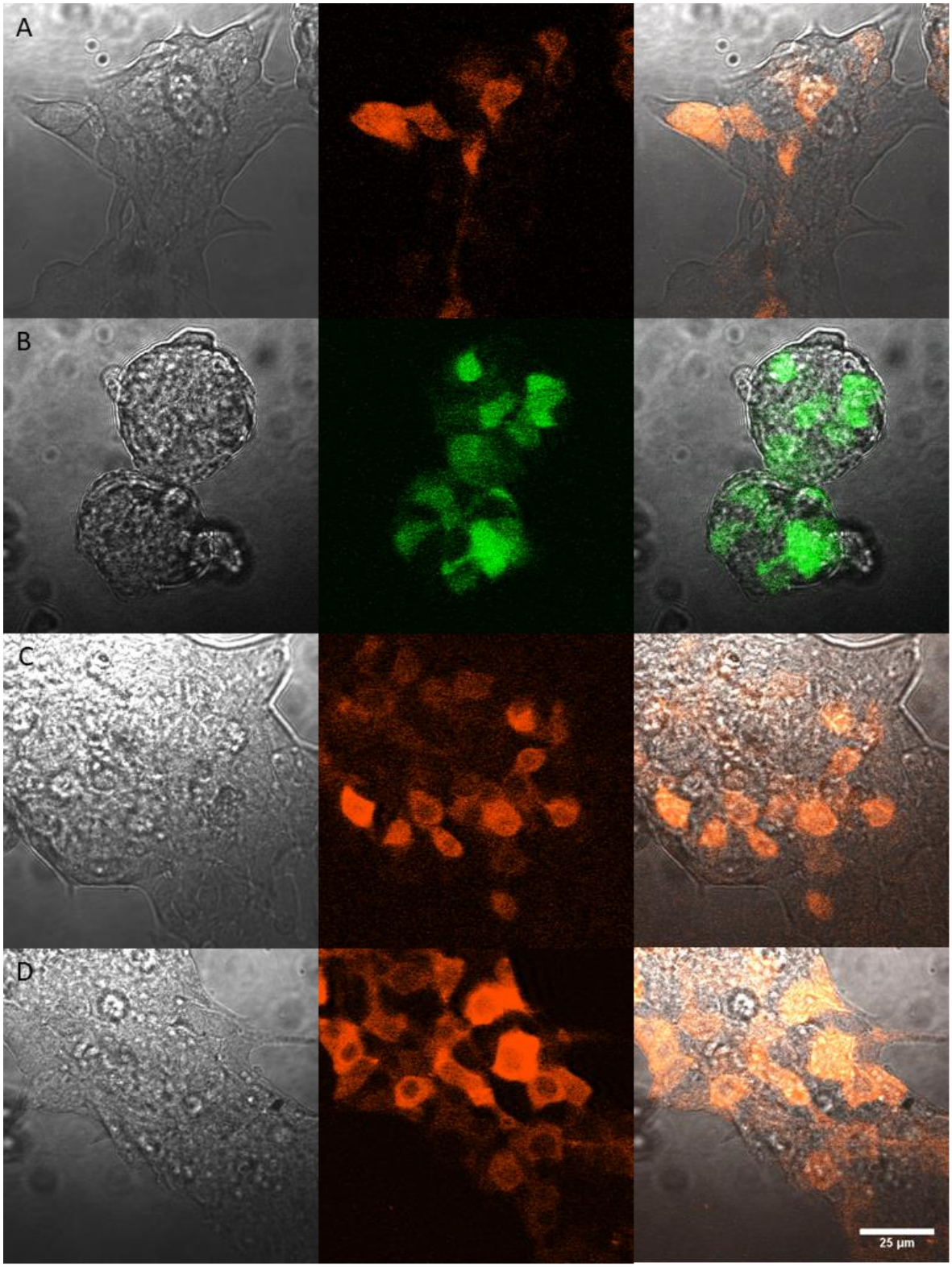

Figure 11 Expression of a viral construct expressing either Mlx/Turbo-RFP (A,C,D) or GFP (B), incubated for 18 hours on either non- (A,B), collagen- (C), or poly-D-lysine- (D) coated plates.

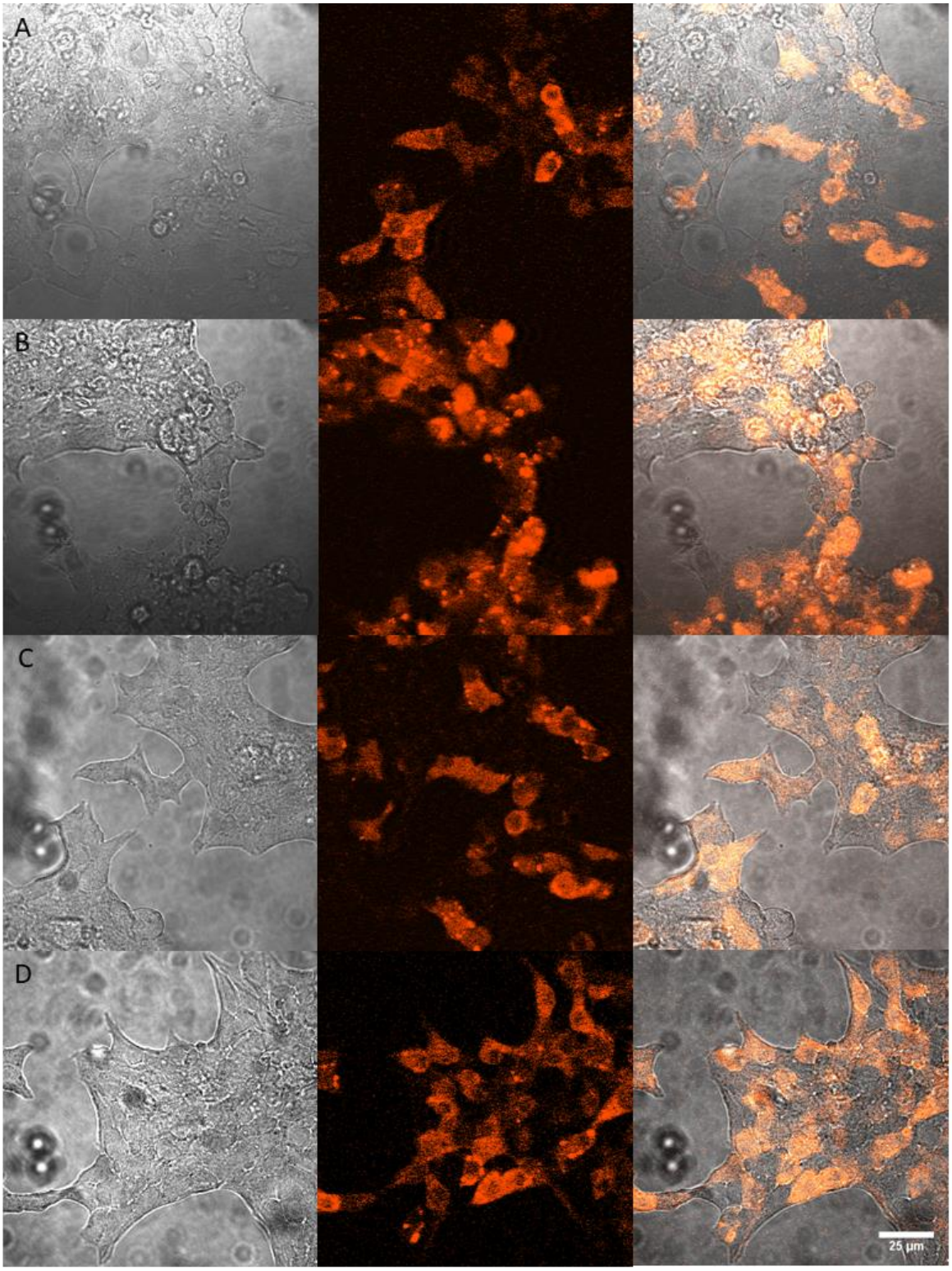

Figure 12 Expression of Mlx/Turbo-RFP in a high (A,B) and a low (C,D) passage INS-1E cell line, incubated for 46 hours with either 0,15 (A); 0.5 (B); 0.2 (C); 0.4 (D) µl virus.

3.3.2 Co-expression of ChREBP and Mlx

A simultaneous overexpression of ChREBP and Mlx was carried out in INS-1E cells, following the protocol described in section 2.2 and 2.3.4. Cells were imaged, using optimal settings for a single image, resulting in a slow acquisition time but a very clear signal. It was observed that that only a small number of cells were expressing both constructs, and the ChREBP was objectively overexpressed in more cells than Mlx (data not shown). Furthermore, even in cases where both viral constructs were expressed, the amount of overexpression varied greatly. Due to these issues imaged cells would have to be carefully selected based on a high level of overexpression in both channels (fig. 13A-C). A sparse number of apoptotic cells were observed, indicating cell viability is not further reduced by the overexpression of an additional construct (data not shown). Excitation of both fluorophores using one excitation wavelength was attempted as described in 2.3.4 (fig. 13D-L). The purpose of this was to obtain a signal from the green and red channel simultaneously hereby being able to use a co-localization analysis and determining a possible binding between ChREBP/Mlx. The emission was collected in two PMT detectors, from 514 to 544 and 580 to 700, using a resonant scanner (fig. 13D-F). A significant signal was observed in both emission filters which indicated that both Mlx and ChREBP could be visualized simultaneously using one excitation wavelength. A control experiment, where only ChREBP or Mlx was overexpressed was conducted using the same parameters as in (fig. 13D-F). Overexpression of ChREBP yielded a significant amount of signal in both the green and red channel (fig. 13G-I), despite lack of Mlx, whereas an overexpression of Mlx yielded no signal in the green channel and almost no signal in the red channel (fig. 13J-L). This indicated that the Mlx signal observed the co-expressed cells were from ChREBP. A different approach was needed to determine binding and diffusion of Mlx and ChREBP.

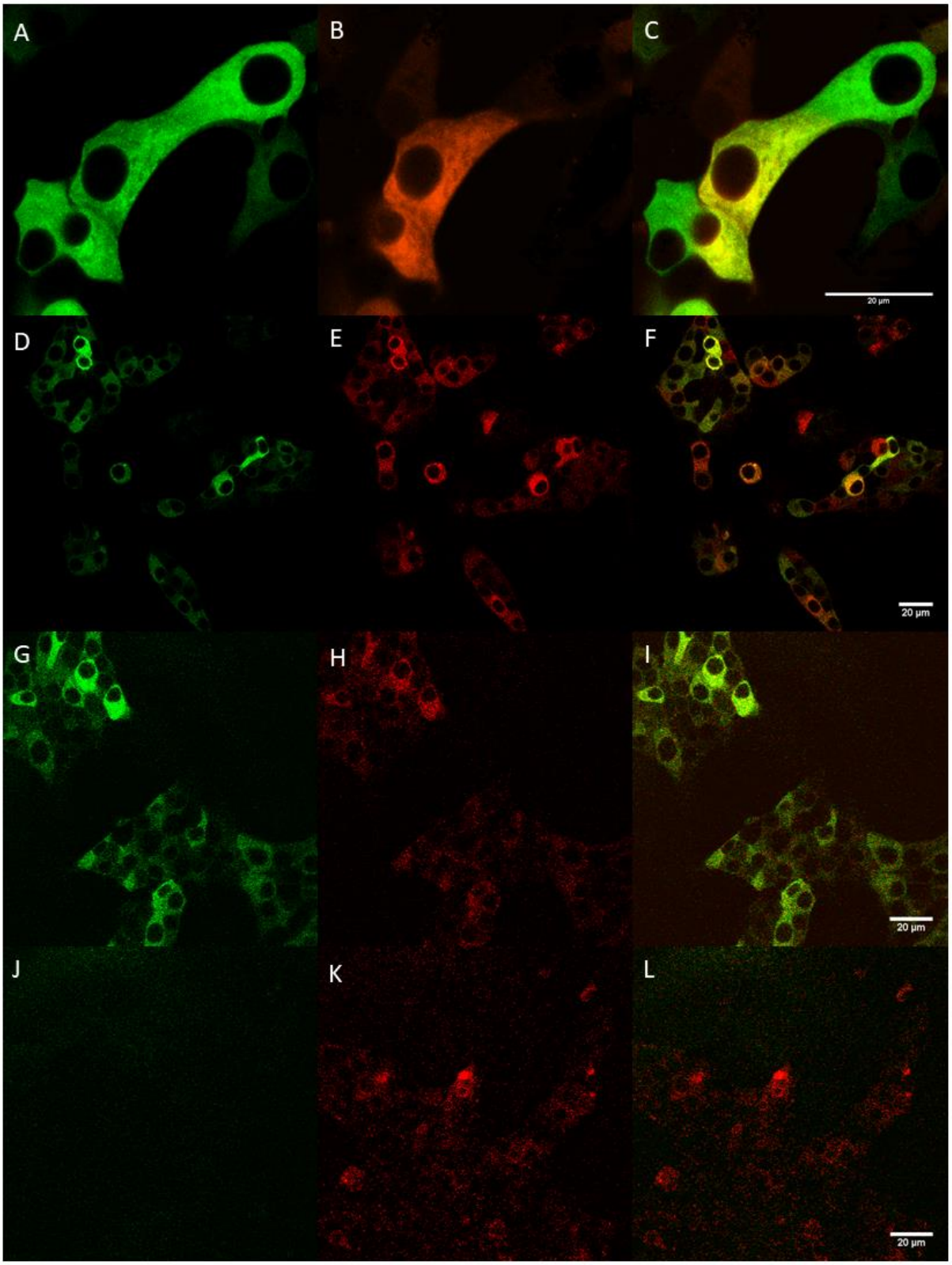

Figure 13 Overexpression of ChREBP (A) and Mlx (B) in a pancreatic beta cell line; INS-1E. A merge of the two channels reveal cells expressing both constructs indicated by yellow (C). Visualization of ChREBP and Mlx in green (D) and red (E) emission channels and merge (F) using a resonant scanner and excitation with a single wavelength. Emission from cells overexpressing either ChREBP (G-I) or Mlx (J-L), in either green (G,J), red (H,K) channel or merge (I,L).

3.4 Quantitative data analysis of ChREBP/Mlx overexpression

A quantitative approach was taken in the analysis of binding capabilities, number of molecules, stoichiometry and diffusion constant from images acquired of cells overexpressing ChREBP and Mlx.

3.4.1 Number & Brightness analysis

A number & brightness analysis was conducted for cells acquired as described in 2.3.4 using a quantitative approach. Images were acquired in a very fast time lapse, using a resonant scanner and analyzed through imageJ using a macro (appendix 7.2). Brightness was calculated during low and high glucose conditions with and without LMB, from time lapses of either the nucleus or the cytoplasm, in cells co-expressing Mlx and ChREBP. Histograms was generated from 3 random regions, which showed a mean intensity during all conditions of approximately 1, indicating that there is no variance in brightness (appendix 7.3). A higher black bar means that more pixel have the same variance as described on the x-axis. From this is can be determined that ChREBP and Mlx does not form oligomers, not even during high glucose conditions and use of a nuclear export inhibitor. Mlx measured in low glucose condition without LMB, interestingly showed a maximum intensity of approximately 2, however the number of particles with this variance was extremely low and not enough to change the mean variance from 1. These high variances are most likely an artifact, due to a bad signal-to-noise ratio.

The number of molecules in focus for each scanned pixel was calculated and the ratio of nuclear and cytoplasmic signal compared, using the same acquired images as for the brightness analysis. Histograms were plotted for 3 random regions in one image, showing the amount of signal each pixel contained during the time lapse (appendix 7.4). Some images contained a different amount of signal in the cytoplasm, likely due to cellular organelles. In these cases, regions were selected from high-signal and low-signal regions. A higher black bar means many pixels have the same number of fluorophores in focus on average. The mean molecules per pixel was plotted, cytoplasmic and nuclear signal assembled in one bar chart, for each condition (fig. 14A-D,F-I). The ratio of nuclear signal versus cytoplasmic signal was calculated by dividing nuclear mean to the cytoplasmic mean (fig. 14E,J). As expected from previous experiments, overexpressed ChREBP was not very present in nucleus during low glucose conditions, but the amount of nuclear ChREBP increased as the glucose concentration was increased approximately 3-fold (fig. 14A,C,E). Inhibition of nuclear export with LMB resulted in an approximate 2.5-3-fold increase in nuclear translocation, relative to untreated cells in low and high glucose respectively (fig. 14E). Treatment with LMB and high glucose yielded that largest nuclear translocation approximately 8.5-fold increase relative to untreated cells in low glucose,

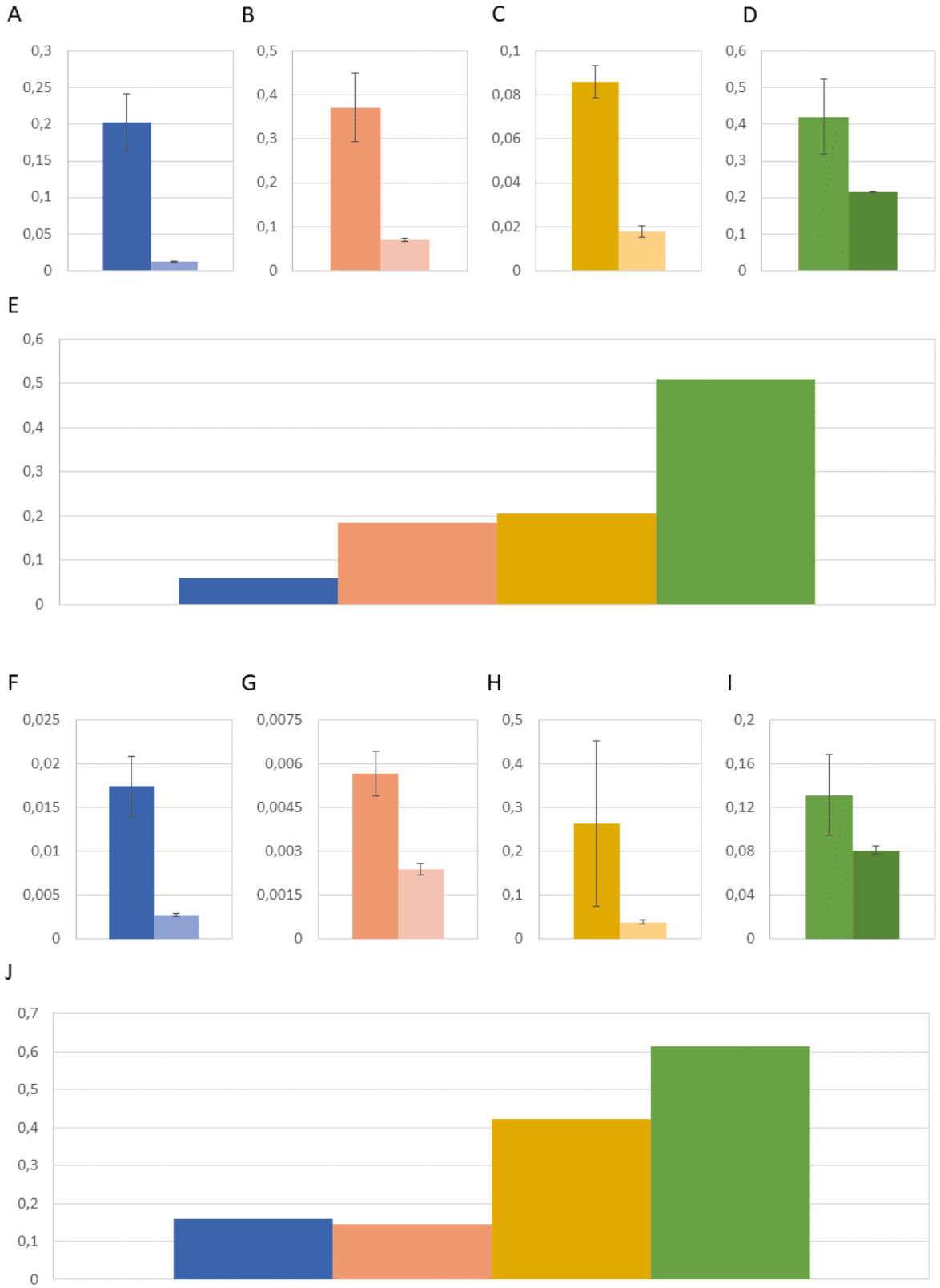

Figure 14 A number analysis yielded a quantification of molecules in each pixel. The amount of signal in cytoplasm (dark color, respectively) is compared to the amount of signal in the nucleus (light color, respectively) in graph A-D and F-I. Overexpression of either ChREBP (A-E) or Mlx (F-J), during 4 different conditions; low (A,B,F,G) or high (C,D,H,I) glucose, without (A,C,F,H) or with (B,D,G,I) LMB, is compared by the nucleus/cytoplasm ratio (E,J). Data and error bars are based on 3 measurements in a single cell.

and 3-fold increase, relative to LMB treated cells in low glucose. The nuclear translocation of overexpressed Mlx was compared as described for ChREBP (fig. 14F-J). Use of LMB did not seem to have an effect on nuclear translocation of Mlx in low glucose condition (fig. 14F,G,J). This might be caused by a very low level of Mlx overexpression in the low glucose and LMB treated cell, which resulted in a fast bleach of every fluorophore in the nucleus. Nuclear translocation from low to high glucose conditions resulted in an approximate 2.5-fold increase of nuclear Mlx (fig. 14F,H,J). A 4-fold higher ratio of nuclear Mlx was measured in the same conditions, when cells were subjected to LMB (fig. 14G,I,J).

No evidence has been found to support a CRM1 mediated nuclear export of Mlx, which also correlates with the observed trend that LMB either has no effect or only a 1.5-fold increase of nuclear Mlx. As is the case for ChREBP, a higher amount of nuclear Mlx is observed in high glucose, relative to low glucose conditions, indicating a nuclear accumulation only dependent on glucose and not LMB. As described in detail in section 1.1-3, ChREBP is highly regulated by phosphorylation and proteins retaining it in the cytoplasm. Glucose metabolites allow Mlx binding and nuclear translocation. It is likely that the higher nuclear translocation of Mlx is caused by ChREBP activation, hereby binding Mlx, mediating its translocation to the nucleus. However, further investigation is needed in order determine if the fraction of translocated Mlx is bound to ChREBP.

3.4.1.1 Investigation of nuclear aggregates

In some cells transfected with both ChREBP and Mlx, certain aggregates containing both fluorophores were observed in the cytoplasm. Interestingly, these aggregates were also observed in cells overexpressing Mlx only, but not in cells overexpressing ChREBP. An example from low glucose and LMB treatment was chosen for a closer investigation. Performing a N&B analysis showed a larger number of ChREBP and Mlx in the assembled aggregate (fig. 15A-B). The aggregate also seemed to show a slightly higher variance, indicating presence of ChREBP or Mlx dimers. This is most likely not the case though, since a N&B analysis is vulnerable to accumulations of protein since the variance can be “artificially” boosted. Nevertheless, the aggregate has a maximum variance of 1.25 and 1.2 for ChREBP and Mlx, respectively, indicating that the proteins most likely exist as monomers. A study by (Kaniuk et al., 2007) has investigated similar structures in pancreatic beta-cells. The study observed aggregates in a similar cell line; INS 832/13, when the cells were subjected to high glucose for a prolonged period. Misfolded or unwanted protein was ubiquitinated and stored in a autophagosome. Due to ubiquitination only occurring during Mlx overexpression, this might be more stressful for the cell than strictly ChREBP overexpression. This might be due to the adenoviral construct being different from the one used for ChREBP overexpression. It might also be because the cell can compensate for a higher than normal level of ChREBP, most likely through phosphorylation of ChREBP rendering it inactive. It is not known whether a similar mechanism exist for inhibiting Mlx.

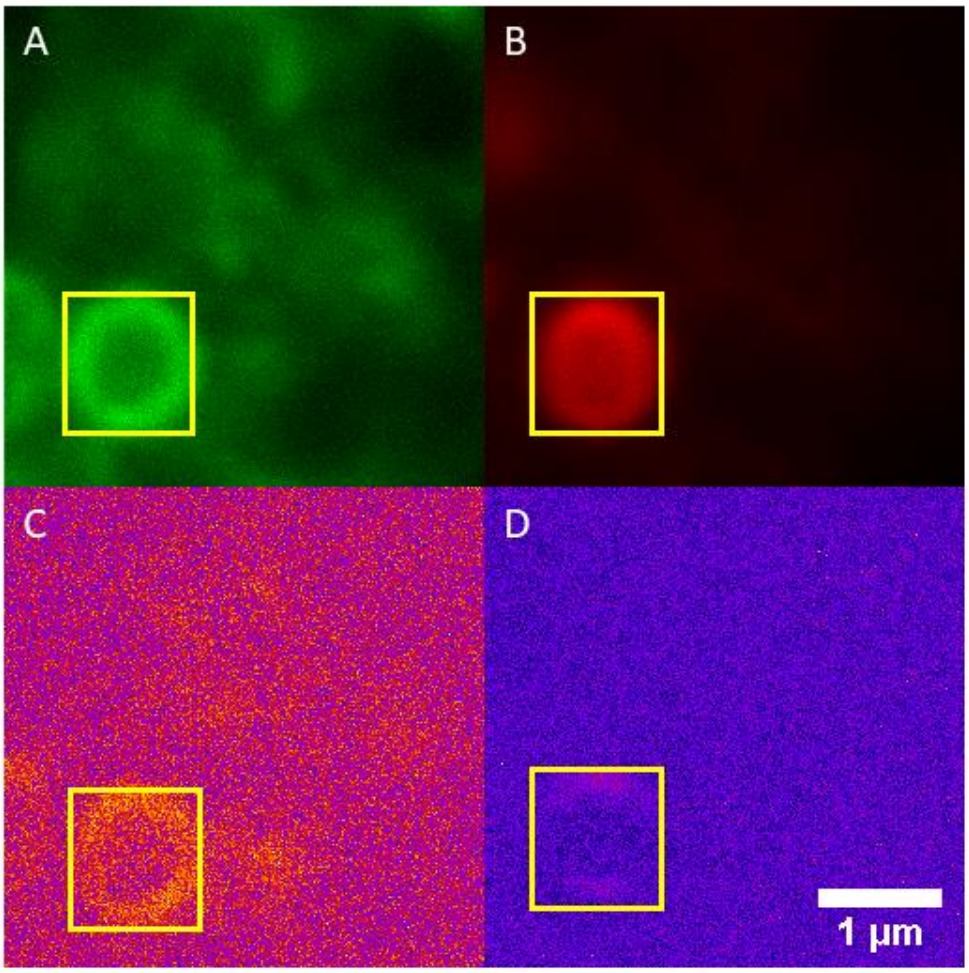

Figure 15 A Number (A,B) and Brightness (C,D) analysis of a cytoplasmic aggregate (yellow box) in a pancreatic beta cell subjected to low glucose condition and LMB treatment, overexpressing ChREBP (A,C) and Mlx (B,D).

3.4.2 TICS

A time lapse of 200 images was acquired as described in section 2.3.4, with a fast scan speed, chosen to reduce bleaching and ensure no movement was lost due to slow scanning. An imageJ plugin named MICS toolkit developed by Chen Chen, Perrine Paul-Gilloteaux and François Waharte, was used to perform a TICS analysis. Diffusion (y) was plotted as the function; y = (a/(1+x/b))+c. The amplitude of the spatial autocorrelation (a), diffusion time (b), offset (c) and spatial autocorrelation to a specific time (x) are calculated using the MICS plugin. The molecular weight of the overexpressed ChREBP-EGFP construct is 128 kDa, which results in a relatively slow estimated diffusion, expected to be around 4 to 8 $\mu m^2/s$ (Nenninger, Mastroianni, & Mullineaux, 2010; Young, Carroad, & Bell, 1980). This estimate might be too high, if there is a fraction of ChREBP-EGFP bound to Mlx or Mlx-TurboRFP. Potential binding of ChREBP and Mlx to chromatin would also lower the diffusion coefficient. The Mlx-TurboRFP construct has a molecular weight of 59 kDa, and the diffusion coefficient is estimated to be slightly faster than ChREBP, at 6 to 10 $\mu m^2/s$. The diffusion coefficient was calculated for 4 conditions; low/high glucose with/without LMB, for both the

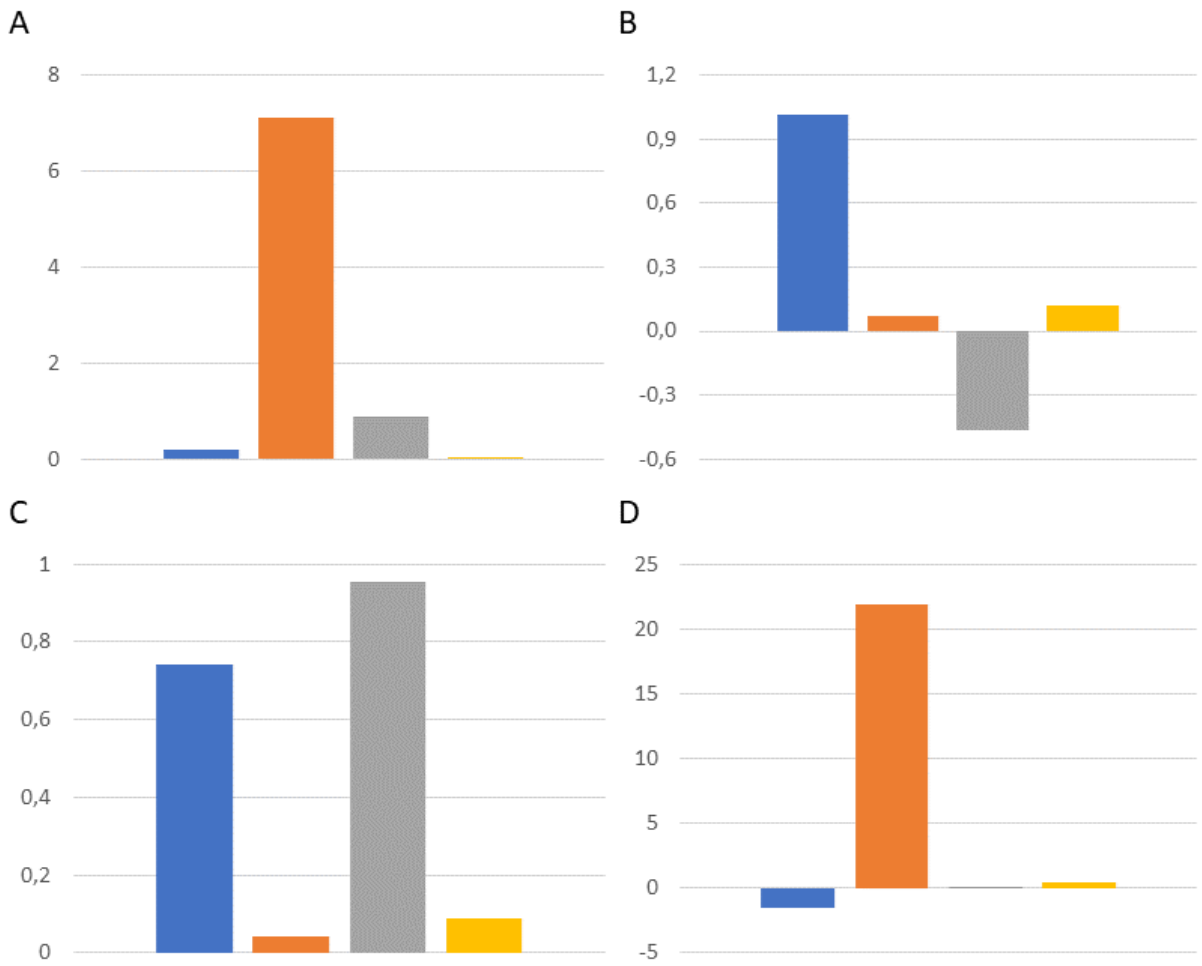

Figure 16 Diffusion coefficients, obtained by TICS analysis of ChREBP (A,B) and Mlx (C,D) in low (blue,orange) and high (grey,yellow) glucose conditions, treated with LMB (orange,yellow), measured in either the cytoplasm (A,C) or nucleus (B,D), in $\mu m^2/s$.

nucleus and cytoplasm (fig. 16). Measured and calculated diffusion coefficents, were in some cases a negative value, which is not possible for a diffusion coefficent. In the worst cases the diffusion coefficent was between 250-fold too low or 1.75-fold too high, relative to the expected diffusion coefficent for ChREBP (fig. 16A,B). Even worse were the diffusion coefficents calculated for Mlx, these were between 500.000-fold too low and 3.5-fold too high (fig. 16C,D). The most likely reason why the TICS analysis did not yield meaningful results, is the scan speed being too fast to obtain enough signal for a good signal-to-noise ratio. Another reason could be that the level of overexpression is not high enough to provide enough signal for this quantitative approach.

A different approach was taken for quantitative analysis of these images using Raster Image Correlation spectroscopy (RICS), which utilizes the linear position change along the x-axis to calculate the difference in time between one pixel and the next. The major difference between TICS and RICS, is the ability of RICS to measure faster diffusion coefficients, the drawback being the requirement of the slower raster scanning. Raster scanning requires the laser to move mono-directionally along the x-axis at a linear speed. A resonant scanner scans bi-directionally along the x-axis at a non-linear speed, which increases the framerate drastically. Additional images were acquired using a HyD detector and a normal albeit slower raster scan, a time lapse was acquired in low and high glucose conditions, in beta cells overexpressing ChREBP. For these data the framerate was approximately 5-fold lower than images used for TICS, due to not using the resonant scanner. Diffusion of nuclear ChREBP was calculated to be 3.7 $\mu m^2/s$ in low glucose and 3.5 $\mu m^2/s$ in high glucose conditions (data not shown). Due to assumptions made for the RICS analysis these numbers should only serve as a general guideline towards calculation of a precise diffusion coefficient. Calculations of RICS diffusion coefficients were performed with help from Dr. Daniel Wüstner.

4. Future experiments

The glucose stimulation procedure consists of manually pipetting a volume of glucose onto the plate while it must remain in focus. This procedure is highly prone to errors, but can be substituted by an automatic plate with a flow from one side to the other, hereby changing the gradient without the risk of changing focus, and enabling a time comparison due to it adding glucose at a very precise time point. Additional replicates should be performed of selective FRAP of ChREBP, in order to determine whether there is a significant difference between rate constants from the slow and fast recovery. Alternatively, this analysis could also be performed on a newer microscope, which will provide a better detection of signal without having to increase laser power, simply due to technical advances. This increased signal might change the rate constants and amplitude observed for cells expressing ChREBP in low glucose conditions where almost no ChREBP is located in the nucleus.

Obtaining additional images for TICS, containing more signal from each fluorophore might result in a more reliable result from this analysis. Alternatively, a RICS analysis can be performed on raster scanned images, comparing the diffusion coefficient from nucleus and cytoplasm, in low and high glucose conditions. Differences in diffusion coefficient could be explained by binding to 14-3-3, sorcin, Mlx or other binding partners. Diffusion of ChREBP and its binding partners could be investigated through purification subsequent measure in a controlled environment. If a comparable difference in diffusion is found, this can be used to determine whether ChREBP is bound to its binding partners just by looking at its diffusion coefficient. In a study by (Chau et al., 2017) an additional binding partner of ChREBP is described; mTORC1, which regulates ChREBP/Mlx translocation to the nucleus. Moreover, mTORC1 is a nutrient and reactive oxygen species sensor, which also controls protein synthesis. The exact mechanism of how mTORC1 regulate ChREBP transcription is yet to be elucidated. Stimulated Emission Depletion (STED) is a microscopy method, which bleaches fluorophores and based on the resulting decrease of signal, can provide a greater resolution than can be resolved through conventional methods. This method is more commonly known as super resolution microscopy, but it requires specific fluorophore to work. Creation of a FLAG-tagged ChREBP enables use of immunofluorescent probes targeted against the FLAG-tag, which means this construct can be visualized through STED microscopy. This would enable high resolution imaging of ChREBP binding to chromatin and subsequent calculation of binding time.

5. Conclusion

A pancreatic beta cell line; INS-1E, was used to investigate the calcium response to glucose stimulation. Calcium oscillations increased by 20 to 30% in a short wave before slowly returning to normal level of oscillation. Removal of extracellular calcium abolished calcium oscillations, but could be rescued by reintroducing extracellular calcium. The transcription factor ChREBP was overexpressed in INS-1E, using a viral construct. ChREBP accumulates in the nucleus during high glucose conditions, removal of extracellular media did not abolish this nuclear accumulation. Nuclear export of ChREBP was blocked using Leptomycin B, a CRM1 inhibitor. A bleaching of nuclear signal in cells overexpressing ChREBP was performed, to quantify the transport across the nuclear membrane, in 4 different conditions; low and high glucose, with and without LMB. Recovery of signal was fit to a bi-exponential function, an immediate fast followed by a slower recovery. The amplitude was calculated and was found to be 2-fold lower in cells treated with LMB, relative to no treatment. A rate constant was calculated for the fast and slow recovery. A pronounced difference was observed for high glucose and LMB treated cells, which exhibited a very low rate constant, relative to untreated in high glucose or low glucose treated and untreated cells. This effect might be caused by the significant nuclear accumulation, preventing more ChREBP from entering the nucleus. Another viral construct was used to overexpress Mlx in combination with ChREBP. The overexpression of Mlx was optimized due to cells detaching from the growth plate due to unknown reasons. A protocol, with longer incubation time and a small amount viral construct, was developed to mitigate the cell detachment. The fluorophores EGFP and TurboRFP, expressed in combination with ChREBP and Mlx, respectively, were not able to be excited simultaneously by a single excitation wavelength. A number & brightness analysis, convincingly suggested that ChREBP and Mlx both exist as monomers, during low and high glucose conditions, with or without treatment with LMB, in both the nucleus and cytoplasm. Aggregates observed in certain conditions were investigated and attributed to ubiquitination of both protein constructs, most likely occurring in autophagosomes. A TICS analysis did not elucidate diffusion coefficients of ChREBP and Mlx constructs, most likely due to a very fast image acquisition time, resulting in very little signal. The diffusion coefficient was able to be estimated using RICS analysis on images acquired through raster scanning, estimating the diffusion of ChREBP to be around 3.5 3.5 $\mu m^2/s$ in the nucleus.

6. References

Aramata, S., Han, S. I., Yasuda, K., & Kataoka, K. (2005). Synergistic activation of the insulin gene promoter by the beta-cell enriched transcription factors MafA, Beta2, and Pdx1. *Biochim Biophys Acta, 1730*(1), 41-46. doi:10.1016/j.bbaexp.2005.05.009

Berridge, M. J., Bootman, M. D., & Roderick, H. L. (2003). Calcium signalling: dynamics, homeostasis and remodelling. *Nat Rev Mol Cell Biol, 4*(7), 517-529. doi:10.1038/nrm1155

Bertram, R., Sherman, A., & Satin, L. S. (2013). Electrical, Calcium, and Metabolic Oscillations in Pancreatic Islets. In M. S. Islam (Ed.), *Islets of Langerhans, 2. ed.* (pp. 1-20). Dordrecht: Springer Netherlands.

Billin, A. N., Eilers, A. L., Queva, C., & Ayer, D. E. (1999). Mlx, a novel Max-like BHLHZip protein that interacts with the Max network of transcription factors. *J Biol Chem, 274*(51), 36344-36350.

Bloom, D., Cafiero, E., Jané-Llopis, E., Abrahams-Gessel, S., Bloom, L., Fathima, S., . . . Weiss, J. (2012). *The Global Economic Burden of Noncommunicable Diseases*. Retrieved from https://EconPapers.repec.org/RePEc:gdm:wpaper:8712

Boergesen, M., Poulsen, L., Schmidt, S. F., Frigerio, F., Maechler, P., & Mandrup, S. (2011). ChREBP mediates glucose repression of peroxisome proliferator-activated receptor alpha expression in pancreatic beta-cells. *J Biol Chem, 286*(15), 13214-13225. doi:10.1074/jbc.M110.215467

Bricambert, J., Miranda, J., Benhamed, F., Girard, J., Postic, C., & Dentin, R. (2010). Salt-inducible kinase 2 links transcriptional coactivator p300 phosphorylation to the prevention of ChREBP-dependent hepatic steatosis in mice. *J Clin Invest, 120*(12), 4316-4331. doi:10.1172/JCI41624

Chau, G. C., Im, D. U., Kang, T. M., Bae, J. M., Kim, W., Pyo, S., . . . Um, S. H. (2017). mTOR controls ChREBP transcriptional activity and pancreatic beta cell survival under diabetic stress. *J Cell Biol, 216*(7), 2091-2105. doi:10.1083/jcb.201701085

da Silva Xavier, G., Rutter, G. A., Diraison, F., Andreolas, C., & Leclerc, I. (2006). ChREBP binding to fatty acid synthase and L-type pyruvate kinase genes is stimulated by glucose in pancreatic beta-cells. *J Lipid Res, 47*(11), 2482-2491. doi:10.1194/jlr.M600289-JLR200

da Silva Xavier, G., Sun, G., Qian, Q., Rutter, G. A., & Leclerc, I. (2010). ChREBP regulates Pdx-1 and other glucose-sensitive genes in pancreatic beta-cells. *Biochem Biophys Res Commun, 402*(2), 252-257. doi:10.1016/j.bbrc.2010.10.010

Davies, M. N., O'Callaghan, B. L., & Towle, H. C. (2008). Glucose activates ChREBP by increasing its rate of nuclear entry and relieving repression of its transcriptional activity. *J Biol Chem, 283*(35), 24029-24038. doi:10.1074/jbc.M801539200

Dentin, R., Benhamed, F., Pegorier, J. P., Foufelle, F., Viollet, B., Vaulont, S., . . . Postic, C. (2005). Polyunsaturated fatty acids suppress glycolytic and lipogenic genes through the inhibition of ChREBP nuclear protein translocation. *J Clin Invest, 115*(10), 2843-2854. doi:10.1172/JCI25256

Dentin, R., Tomas-Cobos, L., Foufelle, F., Leopold, J., Girard, J., Postic, C., & Ferre, P. (2012). Glucose 6-phosphate, rather than xylulose 5-phosphate, is required for the activation of ChREBP in response to glucose in the liver. *J Hepatol, 56*(1), 199-209. doi:10.1016/j.jhep.2011.07.019

Digman, M. A., Dalal, R., Horwitz, A. F., & Gratton, E. (2008). Mapping the number of molecules and brightness in the laser scanning microscope. *Biophys J, 94*(6), 2320-2332. doi:10.1529/biophysj.107.114645

Filhoulaud, G., Guilmeau, S., Dentin, R., Girard, J., & Postic, C. (2013). Novel insights into ChREBP regulation and function. *Trends Endocrinol Metab, 24*(5), 257-268. doi:10.1016/j.tem.2013.01.003

Ge, Q., Nakagawa, T., Wynn, R. M., Chook, Y. M., Miller, B. C., & Uyeda, K. (2011). Importin-alpha protein binding to a nuclear localization signal of carbohydrate response element-binding protein (ChREBP). *J Biol Chem, 286*(32), 28119-28127. doi:10.1074/jbc.M111.237016

Guinez, C., Filhoulaud, G., Rayah-Benhamed, F., Marmier, S., Dubuquoy, C., Dentin, R., . . . Postic, C. (2011). O-GlcNAcylation increases ChREBP protein content and transcriptional activity in the liver. *Diabetes, 60*(5), 1399-1413. doi:10.2337/db10-0452

Havula, E., & Hietakangas, V. (2012). Glucose sensing by ChREBP/MondoA-Mlx transcription factors. *Semin Cell Dev Biol, 23*(6), 640-647. doi:10.1016/j.semcdb.2012.02.007

Kabashima, T., Kawaguchi, T., Wadzinski, B. E., & Uyeda, K. (2003). Xylulose 5-phosphate mediates glucose-induced lipogenesis by xylulose 5-phosphate-activated protein phosphatase in rat liver. *Proc Natl Acad Sci U S A, 100*(9), 5107-5112. doi:10.1073/pnas.0730817100

Kaniuk, N. A., Kiraly, M., Bates, H., Vranic, M., Volchuk, A., & Brumell, J. H. (2007). Ubiquitinated-protein aggregates form in pancreatic beta-cells during diabetes-induced oxidative stress and are regulated by autophagy. *Diabetes, 56*(4), 930-939. doi:10.2337/db06-1160

Kawaguchi, T., Osatomi, K., Yamashita, H., Kabashima, T., & Uyeda, K. (2002). Mechanism for fatty acid "sparing" effect on glucose-induced transcription: regulation of carbohydrate-responsive element-binding protein by AMP-activated protein kinase. *J Biol Chem, 277*(6), 3829-3835. doi:10.1074/jbc.M107895200

Kawaguchi, T., Takenoshita, M., Kabashima, T., & Uyeda, K. (2001). Glucose and cAMP regulate the L-type pyruvate kinase gene by phosphorylation/dephosphorylation of the carbohydrate response element binding protein. *Proc Natl Acad Sci U S A, 98*(24), 13710-13715. doi:10.1073/pnas.231370798

Li, M. V., Chen, W., Harmancey, R. N., Nuotio-Antar, A. M., Imamura, M., Saha, P., . . . Chan, L. (2010). Glucose-6-phosphate mediates activation of the carbohydrate responsive binding protein (ChREBP). *Biochem Biophys Res Commun, 395*(3), 395-400. doi:10.1016/j.bbrc.2010.04.028

Lund, F. W., Lomholt, M. A., Solanko, L. M., Bittman, R., & Wustner, D. (2012). Two-photon time-lapse microscopy of BODIPY-cholesterol reveals anomalous sterol diffusion in chinese hamster ovary cells. *BMC Biophys, 5*, 20. doi:10.1186/2046-1682-5-20

Lund, F. W., & Wustner, D. (2013). A comparison of single particle tracking and temporal image correlation spectroscopy for quantitative analysis of endosome motility. *J Microsc, 252*(2), 169-188. doi:10.1111/jmi.12080

Ma, L., Sham, Y. Y., Walters, K. J., & Towle, H. C. (2007). A critical role for the loop region of the basic helix-loop-helix/leucine zipper protein Mlx in DNA binding and glucose-regulated transcription. *Nucleic Acids Res, 35*(1), 35-44. doi:10.1093/nar/gkl987

Ma, L., Tsatsos, N. G., & Towle, H. C. (2005). Direct role of ChREBP.Mlx in regulating hepatic glucose-responsive genes. *J Biol Chem, 280*(12), 12019-12027. doi:10.1074/jbc.M413063200

Meroni, G., Cairo, S., Merla, G., Messali, S., Brent, R., Ballabio, A., & Reymond, A. (2000). Mlx, a new Max-like bHLHZip family member: the center stage of a novel transcription factors regulatory pathway? *Oncogene, 19*(29), 3266-3277. doi:10.1038/sj.onc.1203634

Minn, A. H., Hafele, C., & Shalev, A. (2005). Thioredoxin-interacting protein is stimulated by glucose through a carbohydrate response element and induces beta-cell apoptosis. *Endocrinology, 146*(5), 2397-2405. doi:10.1210/en.2004-1378

Nenninger, A., Mastroianni, G., & Mullineaux, C. W. (2010). Size dependence of protein diffusion in the cytoplasm of Escherichia coli. *J Bacteriol, 192*(18), 4535-4540. doi:10.1128/JB.00284-10

Nguyen, K. T., Holloway, M. P., & Altura, R. A. (2012). The CRM1 nuclear export protein in normal development and disease. *Int J Biochem Mol Biol, 3*(2), 137-151.

Noordeen, N. A., Meur, G., Rutter, G. A., & Leclerc, I. (2012). Glucose-induced nuclear shuttling of ChREBP is mediated by sorcin and Ca(2+) ions in pancreatic beta-cells. *Diabetes, 61*(3), 574-585. doi:10.2337/db10-1329

Organization, W. H. (2016). *Global report on diabetes*: World Health Organization.

Sakiyama, H., Wynn, R. M., Lee, W. R., Fukasawa, M., Mizuguchi, H., Gardner, K. H., . . . Uyeda, K. (2008). Regulation of nuclear import/export of carbohydrate response element-binding protein (ChREBP): interaction of an alpha-helix of ChREBP with the 14-3-3 proteins and regulation by phosphorylation. *J Biol Chem, 283*(36), 24899-24908. doi:10.1074/jbc.M804308200

Schmidt, S. F., Madsen, J. G., Frafjord, K. O., Poulsen, L., Salo, S., Boergesen, M., . . . Mandrup, S. (2016). Integrative Genomics Outlines a Biphasic Glucose Response and a ChREBP-RORgamma Axis Regulating Proliferation in beta Cells. *Cell Rep, 16*(9), 2359-2372. doi:10.1016/j.celrep.2016.07.063

Semrock.com. https://searchlight.semrock.com/.

Wang, Y., Viscarra, J., Kim, S. J., & Sul, H. S. (2015). Transcriptional regulation of hepatic lipogenesis. *Nat Rev Mol Cell Biol, 16*(11), 678-689. doi:10.1038/nrm4074

Wiseman, P. W., Squier, J. A., Ellisman, M. H., & Wilson, K. R. (2000). Two-photon image correlation spectroscopy and image cross-correlation spectroscopy. *J Microsc, 200*(Pt 1), 14-25.

Xu, J., Christian, B., & Jump, D. B. (2006). Regulation of rat hepatic L-pyruvate kinase promoter composition and activity by glucose, n-3 polyunsaturated fatty acids, and peroxisome proliferator-activated receptor-alpha agonist. *J Biol Chem, 281*(27), 18351-18362. doi:10.1074/jbc.M601277200

Young, M. E., Carroad, P. A., & Bell, R. L. (1980). Estimation of diffusion coefficients of proteins. *Biotechnology and Bioengineering, 22*(5), 947-955. doi:10.1002/bit.260220504

7. Appendix

7.1 Growth and microscope media

M1	Concentration	Mw
NaCl	150 mM	58.44
KCl	5 mM	74.56
$CaCl_2(2H_2O)$	1 mM	147.02
$MgCl_2(6H_2O)$	1 mM	203.30
Glucose(H_2O)	5 mM	198.16
HEPES	20 mM	238.30

RPMI-1640	Concentration	Mw
NaPyruvate	1 mM	110.04
FBS	5 %	-
B-MeOH	50 µM	78.13
Penicillin	100 U/mL	334.39
Streptomycin	100 mg/mL	581.57

Name	Order number	Company
Calcium chloride	C1016	Sigma
Leptomycin B	L2913	Sigma
Fetal Bovine Serum	10270-106	Thermo
RPMI 1640 Medium	11879020 or 61870010	Thermo
35mm glass bottom dishes	P35G-1.5-20-C	Mattek
D-glucose solution (45%)	G8769	Sigma
Fluo-4	F14201	Thermo
Poly-D-lysine	P7886	Sigma
Trypsin-EDTA	t4174	Sigma

7.2 Number & brightness analysis macro

```
var tempo = getTitle;

var AktaDir= getInfo("image.directory");

var SlideNbr=nSlices;

selectWindow(""+tempo+"");

setSlice(1);

run("Z Project...", "projection=[Average Intensity]");

saveAs("Tiff", ""+AktaDir+"\\1stMoment_"+tempo+"");

imageCalculator("Subtract create 32-bit stack", ""+tempo+"","1stMoment_"+tempo+"");

run("Square", "stack");

run("Z Project...", "projection=[Average Intensity]");

saveAs("Tiff", ""+AktaDir+"\\2ndMoment_"+tempo+"");

imageCalculator("Divide create 32-bit","2ndMoment_"+tempo+"","1stMoment_"+tempo+"");

selectWindow("Result of 2ndMoment_"+tempo+"");

saveAs("Tiff", ""+AktaDir+"\\Bmap_"+tempo+"");

selectWindow("1stMoment_"+tempo+"");

run("Square");

imageCalculator("Divide create 32-bit", "1stMoment_"+tempo+"","2ndMoment_"+tempo+"");

selectWindow("Result of 1stMoment_"+tempo+"");

saveAs("Tiff", ""+AktaDir+"\\Nmap_"+tempo+"");
```

7.3 brightness analysis

ChREBP

Low glucose - Cytoplasm

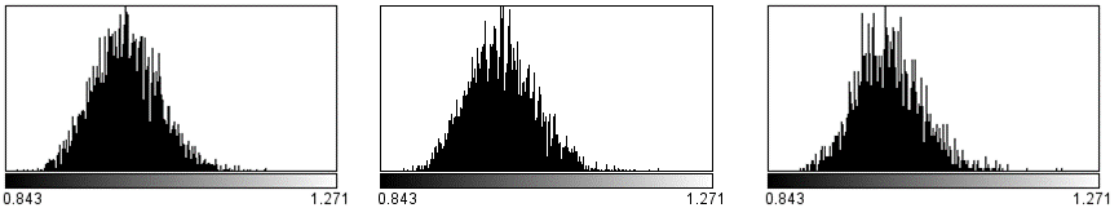

Low glucose - Nucleus

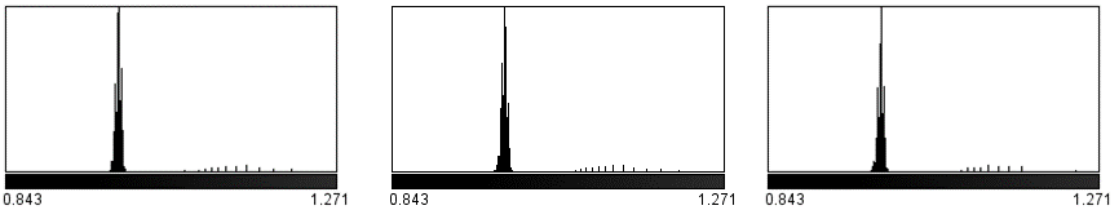

Low glucose LMB - Cytoplasm

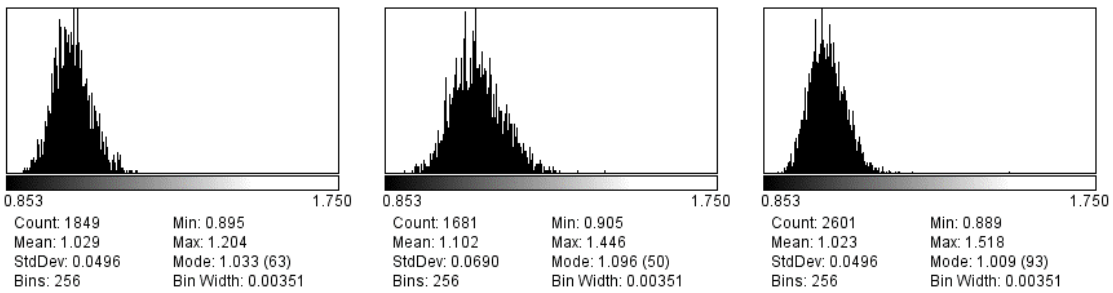

Low glucose LMB - Nucleus

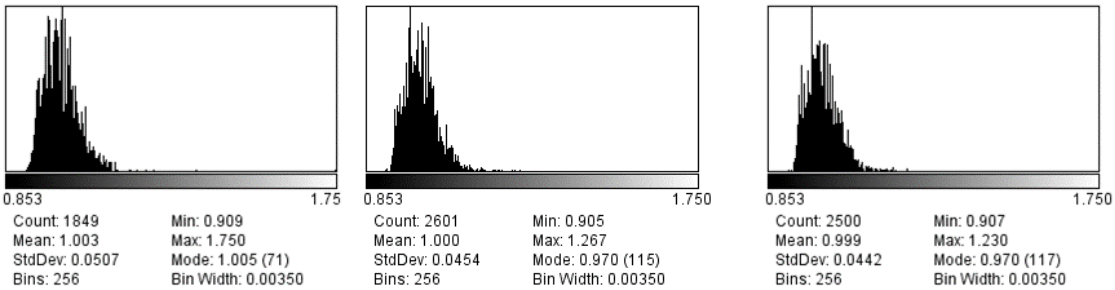

ChREBP

High glucose - Cytoplasm

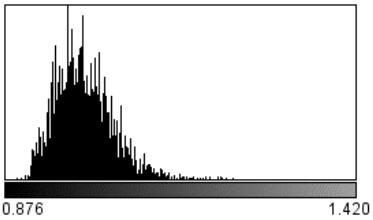

Count: 3844 Min: 0.895
Mean: 0.999 Max: 1.230
StdDev: 0.0459 Mode: 0.973 (109)
Bins: 256 Bin Width: 0.00213

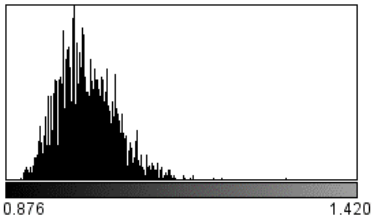

Count: 2601 Min: 0.899
Mean: 1.001 Max: 1.310
StdDev: 0.0456 Mode: 0.981 (71)
Bins: 256 Bin Width: 0.00213

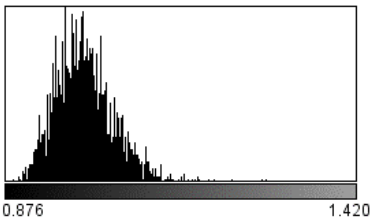

Count: 2809 Min: 0.887
Mean: 0.999 Max: 1.281
StdDev: 0.0454 Mode: 0.968 (71)
Bins: 256 Bin Width: 0.00213

High glucose - Nucleus

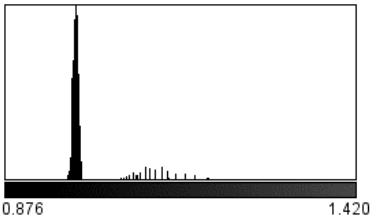

Count: 3842 Min: 0.967
Mean: 1.000 Max: 1.420
StdDev: 0.0458 Mode: 0.985 (633)
Bins: 256 Bin Width: 0.00212

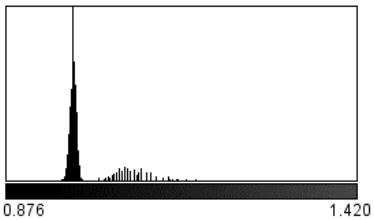

Count: 2809 Min: 0.960
Mean: 0.999 Max: 1.401
StdDev: 0.0432 Mode: 0.979 (509)
Bins: 256 Bin Width: 0.00212

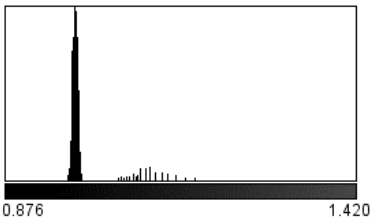

Count: 2599 Min: 0.965
Mean: 0.999 Max: 1.420
StdDev: 0.0431 Mode: 0.983 (419)
Bins: 256 Bin Width: 0.00212

High glucose LMB - Cytoplasm

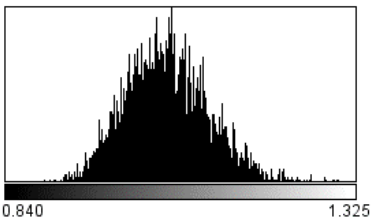

Count: 3969 Min: 0.895
Mean: 1.064 Max: 1.301
StdDev: 0.0587 Mode: 1.070 (67)
Bins: 256 Bin Width: 0.00189

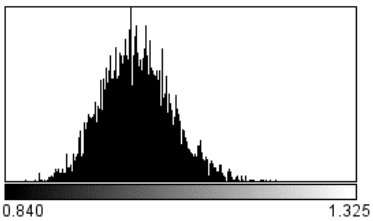

Count: 4096 Min: 0.868
Mean: 1.022 Max: 1.214
StdDev: 0.0491 Mode: 1.013 (83)
Bins: 256 Bin Width: 0.00189

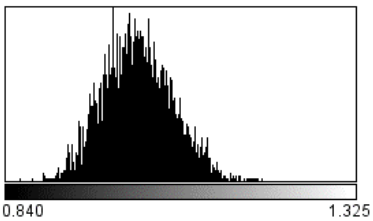

Count: 3249 Min: 0.859
Mean: 1.023 Max: 1.194
StdDev: 0.0490 Mode: 0.989 (60)
Bins: 256 Bin Width: 0.00189

High glucose LMB - Nucleus

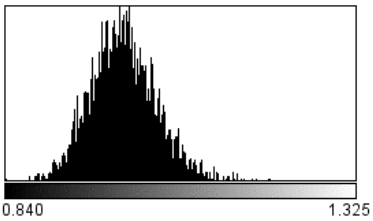

Count: 3844 Min: 0.842
Mean: 1.004 Max: 1.207
StdDev: 0.0459 Mode: 0.998 (76)
Bins: 256 Bin Width: 0.00189

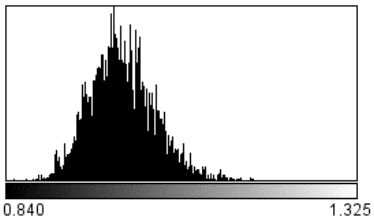

Count: 3969 Min: 0.851
Mean: 1.001 Max: 1.183
StdDev: 0.0461 Mode: 0.989 (87)
Bins: 256 Bin Width: 0.00189

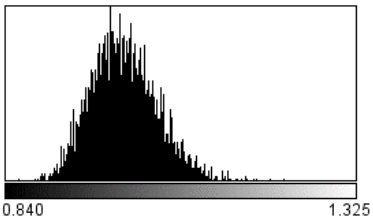

Count: 3481 Min: 0.858
Mean: 1.004 Max: 1.225
StdDev: 0.0461 Mode: 0.985 (71)
Bins: 256 Bin Width: 0.00189

Mlx

Low glucose - Cytoplasm

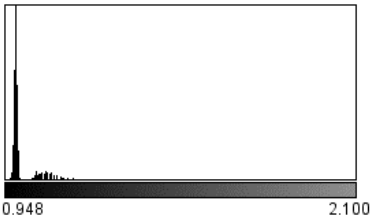

Count: 4624 Min: 0.953
Mean: 1.003 Max: 1.637
StdDev: 0.0502 Mode: 0.982 (1421)
Bins: 256 Bin Width: 0.00450

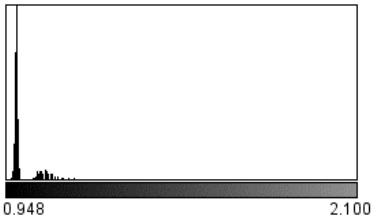

Count: 5040 Min: 0.960
Mean: 1.003 Max: 2.100
StdDev: 0.0496 Mode: 0.982 (1650)
Bins: 256 Bin Width: 0.00450

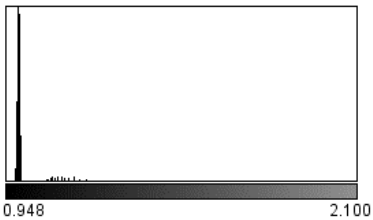

Count: 2208 Min: 0.972
Mean: 1.002 Max: 2.100
StdDev: 0.0549 Mode: 0.986 (729)
Bins: 256 Bin Width: 0.00450

Low glucose - Nucleus

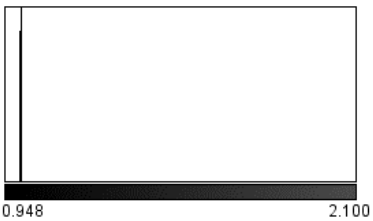

Count: 4141 Min: 0.991
Mean: 1.000 Max: 2.100
StdDev: 0.0381 Mode: 1.000 (2203)
Bins: 256 Bin Width: 0.00450

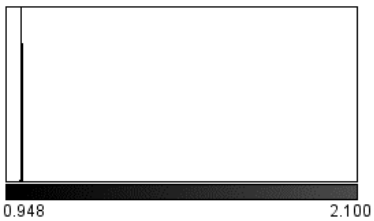

Count: 4726 Min: 0.990
Mean: 0.999 Max: 2.100
StdDev: 0.0263 Mode: 0.995 (2608)
Bins: 256 Bin Width: 0.00450

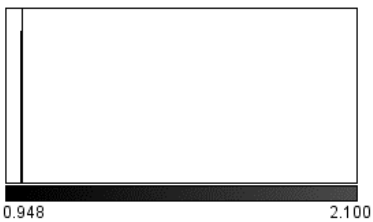

Count: 2014 Min: 0.990
Mean: 0.999 Max: 1.998
StdDev: 0.0370 Mode: 1.000 (1071)
Bins: 256 Bin Width: 0.00450

Low glucose LMB - Cytoplasm

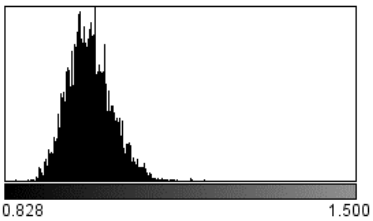

Count: 3844 Min: 0.848
Mean: 0.990 Max: 1.211
StdDev: 0.0438 Mode: 1.000 (111)
Bins: 256 Bin Width: 0.00263

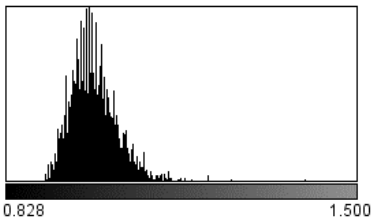

Count: 2601 Min: 0.902
Mean: 0.996 Max: 1.402
StdDev: 0.0454 Mode: 0.987 (89)
Bins: 256 Bin Width: 0.00263

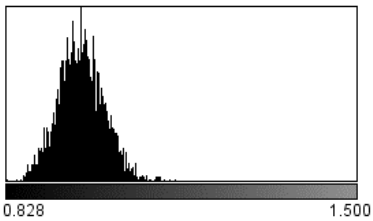

Count: 2809 Min: 0.828
Mean: 0.971 Max: 1.152
StdDev: 0.0445 Mode: 0.971 (84)
Bins: 256 Bin Width: 0.00263

Low glucose LMB - Nucleus

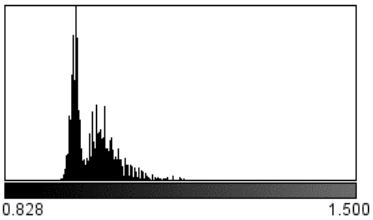

Count: 3136 Min: 0.930
Mean: 0.997 Max: 1.482
StdDev: 0.0444 Mode: 0.963 (237)
Bins: 256 Bin Width: 0.00263

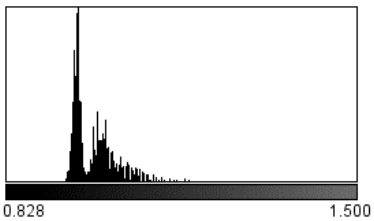

Count: 3248 Min: 0.937
Mean: 0.998 Max: 1.500
StdDev: 0.0452 Mode: 0.966 (281)
Bins: 256 Bin Width: 0.00263

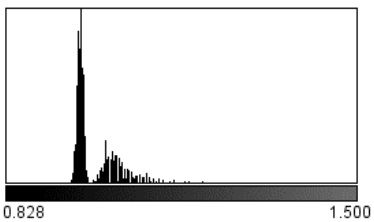

Count: 2401 Min: 0.950
Mean: 0.998 Max: 1.476
StdDev: 0.0467 Mode: 0.971 (283)
Bins: 256 Bin Width: 0.00263

Mlx

High glucose - Cytoplasm

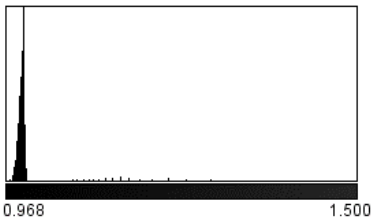

Count: 2600 Min: 0.968
Mean: 0.999 Max: 1.500
StdDev: 0.0404 Mode: 0.994 (606)
Bins: 256 Bin Width: 0.00208

Count: 2664 Min: 0.987
Mean: 0.997 Max: 1.500
StdDev: 0.0208 Mode: 0.994 (1016)
Bins: 256 Bin Width: 0.00208

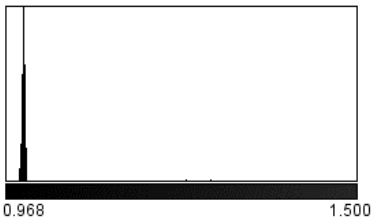

Count: 3010 Min: 0.984
Mean: 0.999 Max: 1.500
StdDev: 0.0391 Mode: 0.994 (1360)
Bins: 256 Bin Width: 0.00208

High glucose - Nucleus

Count: 2728 Min: 0.992
Mean: 0.999 Max: 1.500
StdDev: 0.0231 Mode: 0.998 (1443)
Bins: 256 Bin Width: 0.00208

Count: 2337 Min: 0.990
Mean: 0.998 Max: 1.500
StdDev: 0.0132 Mode: 0.998 (1448)
Bins: 256 Bin Width: 0.00208

Count: 2186 Min: 0.992
Mean: 0.998 Max: 1.500
StdDev: 0.0107 Mode: 0.998 (1470)
Bins: 256 Bin Width: 0.00208

High glucose LMB - Cytoplasm

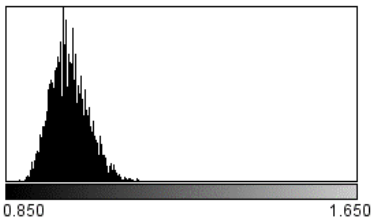

Count: 3844 Min: 0.879
Mean: 0.994 Max: 1.274
StdDev: 0.0450 Mode: 0.980 (150)
Bins: 256 Bin Width: 0.00312

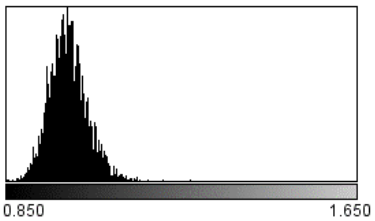

Count: 3481 Min: 0.852
Mean: 0.992 Max: 1.270
StdDev: 0.0439 Mode: 0.989 (120)
Bins: 256 Bin Width: 0.00312

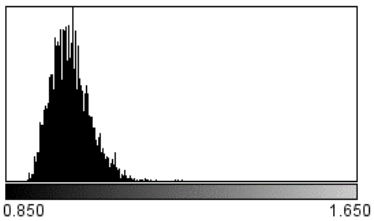

Count: 2704 Min: 0.898
Mean: 0.997 Max: 1.251
StdDev: 0.0456 Mode: 1.002 (95)
Bins: 256 Bin Width: 0.00312

High glucose LMB - Nucleus

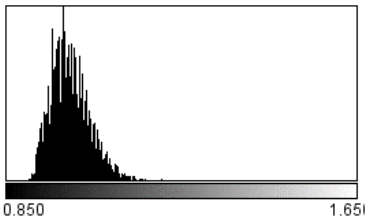

Count: 5184 Min: 0.893
Mean: 0.996 Max: 1.336
StdDev: 0.0451 Mode: 0.979 (200)
Bins: 256 Bin Width: 0.00312

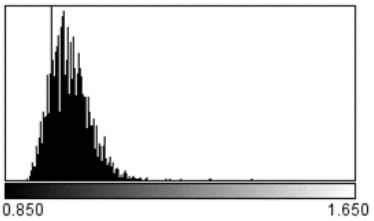

Count: 2916 Min: 0.899
Mean: 0.997 Max: 1.414
StdDev: 0.0466 Mode: 0.954 (107)
Bins: 256 Bin Width: 0.00312

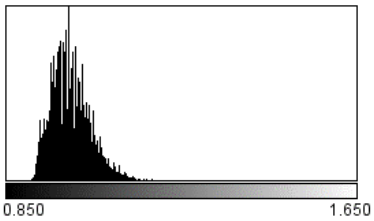

Count: 3844 Min: 0.908
Mean: 0.998 Max: 1.256
StdDev: 0.0456 Mode: 0.992 (158)
Bins: 256 Bin Width: 0.00312

7.4 Number analysis

ChREBP

Low glucose - Cytoplasm

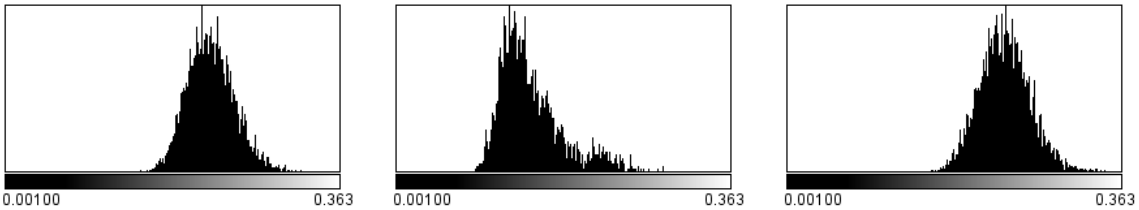

Low glucose - Nucleus

Low glucose LMB - Cytoplasm

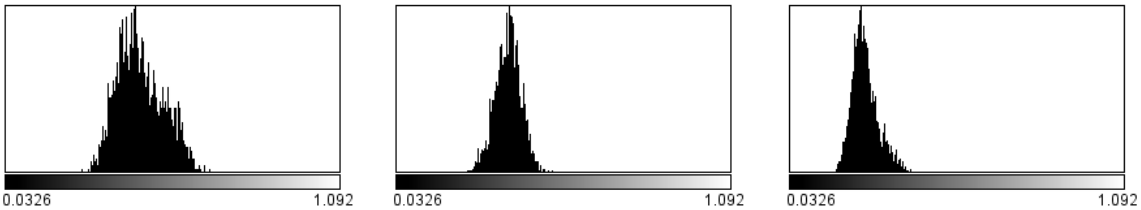

Low glucose LMB - Nucleus

ChREBP

High glucose - Cytoplasm

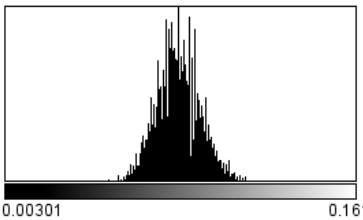

Count: 3844 Min: 0.0462
Mean: 0.0810 Max: 0.117
StdDev: 0.00989 Mode: 0.0810 (130)
Bins: 256 Bin Width: 0.000617

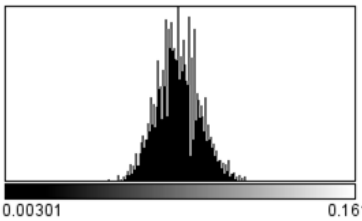

Count: 3844 Min: 0.0462
Mean: 0.0810 Max: 0.117
StdDev: 0.00989 Mode: 0.0810 (130)
Bins: 256 Bin Width: 0.000617

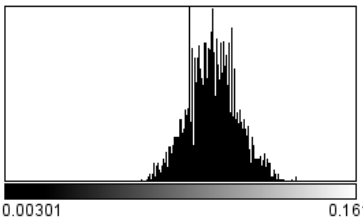

Count: 2601 Min: 0.0641
Mean: 0.0965 Max: 0.134
StdDev: 0.0112 Mode: 0.0860 (76)
Bins: 256 Bin Width: 0.000617

High glucose - Nucleus

Count: 3844 Min: 0.00402
Mean: 0.0154 Max: 0.0341
StdDev: 0.00421 Mode: 0.0132 (381)
Bins: 256 Bin Width: 0.000617

Count: 2601 Min: 0.00301
Mean: 0.0164 Max: 0.0363
StdDev: 0.00422 Mode: 0.0163 (243)
Bins: 256 Bin Width: 0.000617

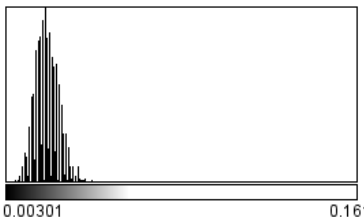

Count: 2809 Min: 0.00604
Mean: 0.0212 Max: 0.0418
StdDev: 0.00531 Mode: 0.0206 (218)
Bins: 256 Bin Width: 0.000617

High glucose LMB - Cytoplasm

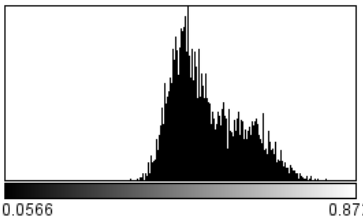

Count: 3969 Min: 0.347
Mean: 0.528 Max: 0.802
StdDev: 0.0819 Mode: 0.482 (98)
Bins: 256 Bin Width: 0.00318

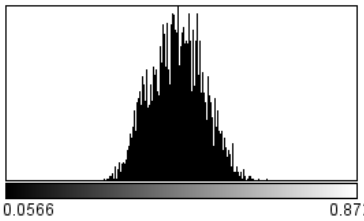

Count: 3249 Min: 0.286
Mean: 0.454 Max: 0.664
StdDev: 0.0622 Mode: 0.456 (74)
Bins: 256 Bin Width: 0.00318

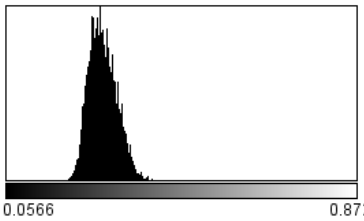

Count: 4096 Min: 0.193
Mean: 0.281 Max: 0.397
StdDev: 0.0325 Mode: 0.275 (172)
Bins: 256 Bin Width: 0.00318

High glucose LMB - Nucleus

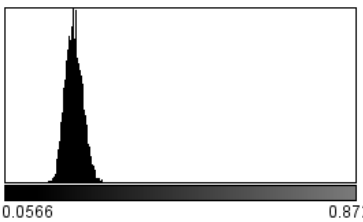

Count: 3844 Min: 0.154
Mean: 0.216 Max: 0.299
StdDev: 0.0205 Mode: 0.214 (260)
Bins: 256 Bin Width: 0.00319

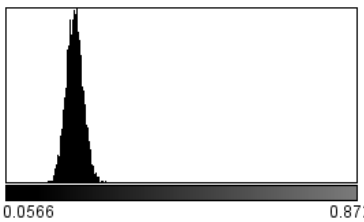

Count: 3481 Min: 0.155
Mean: 0.215 Max: 0.288
StdDev: 0.0199 Mode: 0.221 (228)
Bins: 256 Bin Width: 0.00319

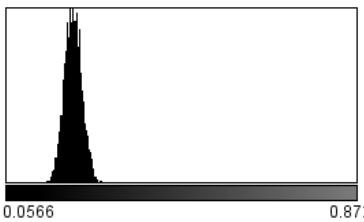

Count: 3969 Min: 0.127
Mean: 0.212 Max: 0.289
StdDev: 0.0204 Mode: 0.211 (245)
Bins: 256 Bin Width: 0.00319

Mlx

Low glucose - Cytoplasm

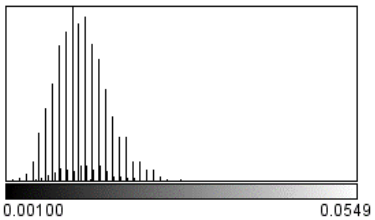

Count: 2209 Min: 0.00200
Mean: 0.0126 Max: 0.0288
StdDev: 0.00398 Mode: 0.0112 (219)
Bins: 256 Bin Width: 0.000211

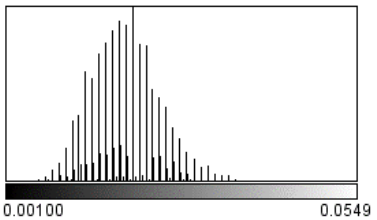

Count: 4624 Min: 0.00358
Mean: 0.0193 Max: 0.0493
StdDev: 0.00531 Mode: 0.0205 (333)
Bins: 256 Bin Width: 0.000211

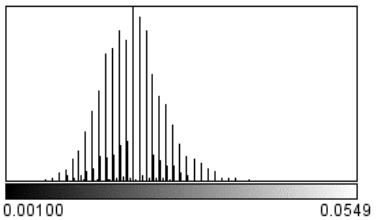

Count: 5041 Min: 0.00644
Mean: 0.0203 Max: 0.0417
StdDev: 0.00482 Mode: 0.0205 (412)
Bins: 256 Bin Width: 0.000211

Low glucose - Nucleus

Count: 2014 Min: 0.00100
Mean: 0.00265 Max: 0.0101
StdDev: 0.00146 Mode: 0.00195 (576)
Bins: 256 Bin Width: 0.000211

Count: 4142 Min: 0.00100
Mean: 0.00261 Max: 0.00908
StdDev: 0.00141 Mode: 0.00195 (1177)
Bins: 256 Bin Width: 0.000211

Count: 4727 Min: 0.00100
Mean: 0.00300 Max: 0.0101
StdDev: 0.00156 Mode: 0.00195 (1234)
Bins: 256 Bin Width: 0.000211

Low glucose LMB - Cytoplasm

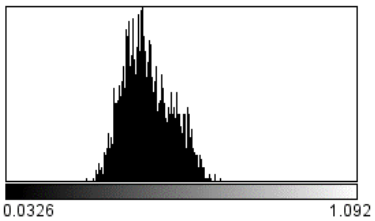

Count: 1681 Min: 0.275
Mean: 0.460 Max: 0.679
StdDev: 0.0732 Mode: 0.444 (47)
Bins: 256 Bin Width: 0.00414

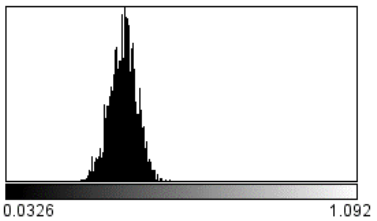

Count: 1849 Min: 0.260
Mean: 0.386 Max: 0.526
StdDev: 0.0410 Mode: 0.390 (88)
Bins: 256 Bin Width: 0.00414

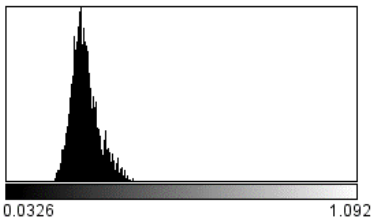

Count: 2601 Min: 0.152
Mean: 0.270 Max: 0.438
StdDev: 0.0419 Mode: 0.258 (136)
Bins: 256 Bin Width: 0.00414

Low glucose LMB - Nucleus

Count: 2401 Min: 0.0111
Mean: 0.0318 Max: 0.0596
StdDev: 0.00617 Mode: 0.0298 (443)
Bins: 256 Bin Width: 0.00276

Count: 3136 Min: 0.0183
Mean: 0.0423 Max: 0.0765
StdDev: 0.00850 Mode: 0.0408 (486)
Bins: 256 Bin Width: 0.00276

Count: 3249 Min: 0.0183
Mean: 0.0398 Max: 0.0672
StdDev: 0.00722 Mode: 0.0408 (537)
Bins: 256 Bin Width: 0.00276

Mlx

High glucose - Cytoplasm

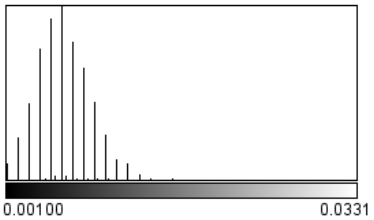

Count: 3015 Min: 0.00100
Mean: 0.00621 Max: 0.0163
StdDev: 0.00249 Mode: 0.00608 (501)
Bins: 256 Bin Width: 0.000125

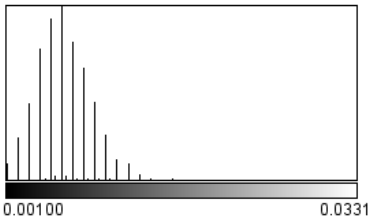

Count: 3015 Min: 0.00100
Mean: 0.00621 Max: 0.0163
StdDev: 0.00249 Mode: 0.00607 (501)
Bins: 256 Bin Width: 0.000125

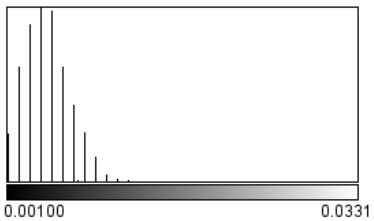

Count: 2667 Min: 0.00100
Mean: 0.00456 Max: 0.0132
StdDev: 0.00209 Mode: 0.00407 (489)
Bins: 256 Bin Width: 0.000125

High glucose - Nucleus

Count: 2340 Min: 0.00100
Mean: 0.00234 Max: 0.0101
StdDev: 0.00129 Mode: 0.00106 (729)
Bins: 256 Bin Width: 0.000125

Count: 2188 Min: 0.00100
Mean: 0.00218 Max: 0.00806
StdDev: 0.00118 Mode: 0.00106 (761)
Bins: 256 Bin Width: 0.000125

Count: 2729 Min: 0.00100
Mean: 0.00265 Max: 0.00806
StdDev: 0.00144 Mode: 0.00194 (777)
Bins: 256 Bin Width: 0.000125

High glucose LMB - Cytoplasm

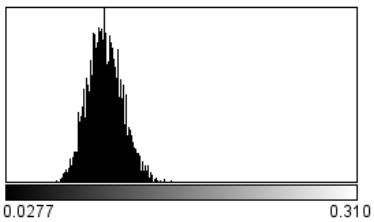

Count: 3844 Min: 0.0616
Mean: 0.107 Max: 0.167
StdDev: 0.0143 Mode: 0.107 (138)
Bins: 256 Bin Width: 0.00110

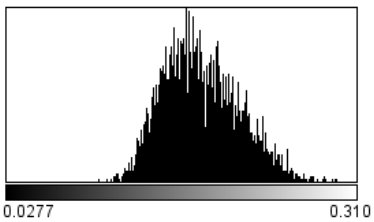

Count: 3481 Min: 0.102
Mean: 0.184 Max: 0.294
StdDev: 0.0307 Mode: 0.173 (63)
Bins: 256 Bin Width: 0.00110

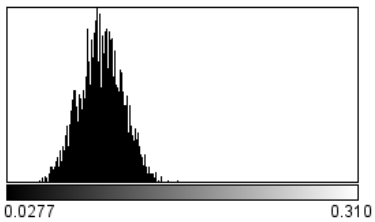

Count: 2704 Min: 0.0540
Mean: 0.103 Max: 0.165
StdDev: 0.0174 Mode: 0.0999 (81)
Bins: 256 Bin Width: 0.00110

High glucose LMB - Nucleus

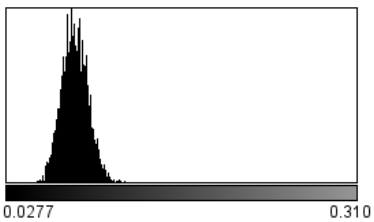

Count: 5184 Min: 0.0489
Mean: 0.0828 Max: 0.123
StdDev: 0.0107 Mode: 0.0801 (236)
Bins: 256 Bin Width: 0.00110

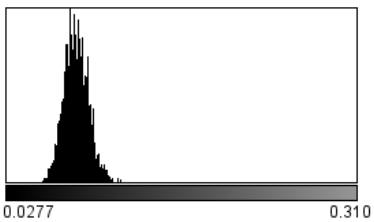

Count: 2916 Min: 0.0494
Mean: 0.0839 Max: 0.124
StdDev: 0.0100 Mode: 0.0790 (146)
Bins: 256 Bin Width: 0.00110

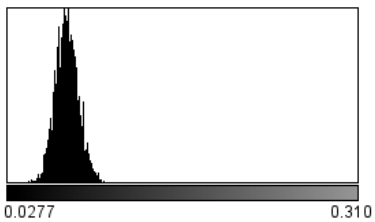

Count: 3844 Min: 0.0449
Mean: 0.0755 Max: 0.111
StdDev: 0.00947 Mode: 0.0735 (193)
Bins: 256 Bin Width: 0.00110